

Universal spin-resolved thermal radiation laws for nonreciprocal bianisotropic media

Chinmay Khandekar,^{1,*} Farhad Khosravi,² Zhou Li,¹ and Zubin Jacob^{1,†}

¹*Birck Nanotechnology Center, School of Electrical and Computer Engineering, College of Engineering, Purdue University, West Lafayette, Indiana 47907, USA*

²*Department of Electrical and Computer Engineering, University of Alberta, Edmonton, Alberta T6G1H9, Canada*

(Dated: June 11, 2020)

A chiral absorber of light can emit spin-polarized (circularly polarized) thermal radiation based on Kirchhoff's law which equates spin-resolved emissivity with spin-resolved absorptivity for reciprocal media at thermal equilibrium. No such law is known for nonreciprocal media. In this work, we discover three spin-resolved Kirchhoff's laws of thermal radiation applicable for both reciprocal and nonreciprocal planar media. In particular, these laws are applicable to multi-layered or composite slabs of generic bianisotropic material classes which include (uniaxial or biaxial) birefringent crystals, (gyrotropic) Weyl semimetals, magnetized semiconductors, plasmas, ferromagnets and ferrites, (magnetoelectric) topological insulators, metamaterials and multiferroic media. We also propose an experiment to verify these laws using a single system of doped Indium Antimonide (InSb) thin film in an external magnetic field. Furthermore, we reveal a surprising result that the planar slabs of all these material classes can emit partially circularly polarized thermal light without requiring any surface patterning, and identify planar configurations which can experience nontrivial thermal optomechanical forces and torques upon thermal emission into the external environment at lower temperature (nonequilibrium). Our work also provides a new fundamental insight of detailed balance of angular momentum (in addition to energy) of equilibrium thermal radiation, and paves the way for practical functionalities based on thermal radiation using nonreciprocal bianisotropic materials.

I. INTRODUCTION

At the foundation of the field of thermal radiation lies Kirchhoff's law which relates emissivity with absorptivity. One formulation of Kirchhoff's law in the context of circularly polarized light states that emissivity (η) is equal to absorptivity (α) for both left circular polarization (LCP) and right circular polarization (RCP) states. Its mathematical form is:

$$\eta_{(+,-)}(\omega, \mathbf{n}) = \alpha_{(+,-)}(\omega, \mathbf{n})$$

where (+) denotes RCP, (-) denotes LCP, ω is the frequency and \mathbf{n} denotes the direction. However, this spin-resolved Kirchhoff's law is valid only for reciprocal media. Many works have used it to design reciprocal chiral absorbers [1–3] which can emit partially spin-polarized thermal radiation and few works have demonstrated it in experiments [4, 5]. This conventional law is not applicable for nonreciprocal media with broken time reversal symmetry such as semiconductors in external magnetic fields. Naturally, the question then arises whether new forms of Kirchhoff's laws exist [6]. In this work, we provide the spin-resolved Kirchhoff's laws which are applicable for nonreciprocal media.

Thermal radiation from nonreciprocal media is an emerging research area [7–11]. There are no experiments till date and computational tools for analyzing nonreciprocal thermal radiation in arbitrary geometries are still under development [12, 13]. While the recent interesting works primarily investigate the heat flux, we introduce a different perspective of spin-resolved or spin-polarized radiative heat flux, which is partially

motivated by the well-known concept of electronic spin currents in condensed matter physics [14]. In our recent work [15], we comprehensively analyze the spin of thermal radiation in the *near-field* of generic nonreciprocal media. We show interesting effects like persistent radiative heat current and persistent photon spin that can exist in the near-field without any temperature difference and explain their connection with the spin-momentum locking of evanescent photonic states [16]. Here, we provide a similar comprehensive analysis in the *far-field* of nonreciprocal media.

We derive the spin-resolved emissivities and absorptivities for planar media using the radiometry principles and based on fluctuational electrodynamic calculations [15]. Our derivation is applicable for both reciprocal and nonreciprocal media because it does not require the concept of electromagnetic reciprocity. We further validate this derivation by proving thermodynamic consistency based on the detailed balance of linear and angular momentum transfer, via thermal radiation between the planar slab and the environment at thermal equilibrium. The spin-resolved emissivities and absorptivities ensure that there is no nonzero force (linear momentum balance) or torque (angular momentum balance) on the planar slab when it is at thermal equilibrium with the environment.

The principle of detailed balance of energy plays a pivotal role in the derivation of many heat-transfer laws. Here, we introduce a new concept of detailed balance of angular momentum of radiative heat at thermal equilibrium. Since this concept is generalizable to electrons, phonons, photons in various systems, it

represents a paradigm shift in the analysis of heat transfer at thermal equilibrium. In this work, it is crucial for validating the spin-resolved emissivities for nonreciprocal media which have not been derived previously.

We then analyze the spin-resolved thermal emission and absorption for planar media of all time-invariant bianisotropic material classes. The reciprocal media include uni/biaxial anisotropic materials [17] and reciprocal magnetoelectric (chiral) media [18, 19], apart from commonly considered isotropic dielectric and metallic materials. The nonreciprocal materials include gyroelectric media like metals and semiconductors in magnetic field [20–22] and Weyl semimetals [23], gyromagnetic media like ferromagnets and ferrites [24], and nonreciprocal magnetoelectric media like multiferroics [25], topological insulators [26] and magnetoelectric heterostructures [27]. The universal spin-resolved analysis of these material classes leads us to discover three spin-resolved Kirchhoff's laws (**SKLs**) which provide useful relations between the spin-resolved emissivities and absorptivities. While the first law for the reciprocal media is intuitively expected, the other two laws for the nonreciprocal media are new. They demonstrate a subtle balance of spin-resolved emission and absorption of thermal radiation, which maintains thermal equilibrium of the non-reciprocal planar media with the surrounding. We emphasize that these laws are applicable for composite or multi-layered configurations of these materials for all frequencies, emission directions, material and geometry parameters. We further propose an experiment which can validate these laws conveniently using a single material system of a doped InSb thin film in the presence of magnetic field.

Apart from the Kirchhoff's laws derived at thermal equilibrium, we also reveal other interesting spin-resolved thermal radiation features observed when the external environment is at lower temperature (nonequilibrium condition). First, we point out a striking result that the planar geometries of all material classes mentioned above except the conventional isotropic dielectric/metallic materials can emit partially spin-polarized thermal radiation in suitable directions. This is important from the perspective of generating circularly polarized light because most of these materials do not require any surface patterning which otherwise causes additional design complexity in previous experiments [4, 5]. Second, we show that the planar slabs can experience nonequilibrium force and torque due to the loss of linear momentum and angular momentum respectively via thermal emission. We discuss their directionalities for all material classes so that both parallel and perpendicular components of the thermal-nonequilibrium optomechanical forces and torques can be engineered using multi-layered planar slabs.

All these findings and theory details will be useful

for engineering directional radiative heat transfer [7, 15] for optimized energy harvesting [28], designing novel spin-polarized LEDs [29], tailoring thermal optomechanical forces and torques [30, 31], and classifying or identifying materials based on infrared polarimetry. Fundamentally, our work simultaneously advances many research topics like thermal radiation, photon spin and angular momentum, electromagnetic nonreciprocity, bianisotropic media and metamaterials, optical characterization of materials etcetera.

II. RESULTS

A. Spin-resolved Kirchhoff's laws

We consider an extended finite-thickness multilayered planar slab much larger than the thermal wavelength at thermal equilibrium with the blackbody radiation at temperature T . As shown in fig.1(a), the power emitted per unit surface area (dA) of the body at an angle θ to the surface normal within the solid angle $d\Omega$ per unit frequency interval ($d\omega$) is given by,

$$P_{\text{rad}}(\omega, \theta, \phi, \hat{\mathbf{e}}) = \eta(\omega, \theta, \phi, \hat{\mathbf{e}}) \frac{I_b(\omega, T)}{2} \cos \theta d\omega d\Omega dA \quad (1)$$

where η is the dimensionless emissivity dependent on frequency (ω), emission direction (θ, ϕ) in spherical coordinates and orthogonal polarization states ($\hat{\mathbf{e}}$). The angle $\phi \in [0, 2\pi]$ while the angle $\theta \in [0, \pi]$ such that $\theta \in [0, \pi/2]$ denotes the top hemisphere and $\theta \in [\pi/2, \pi]$ denotes the bottom hemisphere. For a semi-infinite half-space, $\theta \in [0, \pi/2]$. The blackbody radiance at temperature T given by $I_b(\omega, T) = \omega^2 \Theta(\omega, T) / (4\pi^3 c^2)$ with $\Theta(\omega, T) = \hbar\omega / [\exp(\hbar\omega/k_B T) - 1]$ being the Planck's function, is divided by two to account for two polarization states separately. Similarly, the power absorbed per unit surface area dA due to the blackbody radiance incident at an angle θ to the surface normal within a solid angle $d\Omega$ per unit frequency interval $d\omega$ is,

$$P_{\text{abs}}(\omega, \theta, \phi, \hat{\mathbf{e}}) = \alpha(\omega, \theta, \phi, \hat{\mathbf{e}}) \frac{I_b(\omega, T)}{2} \cos \theta d\omega d\Omega dA \quad (2)$$

We focus on polarization-dependent properties of thermal emission. Instead of the usual s, p -polarization basis, we consider RCP ($\hat{\mathbf{e}}_+$) and LCP ($\hat{\mathbf{e}}_-$) polarization states. The circular polarization basis states in the basis of s, p polarization states ($\hat{\mathbf{e}}_s, \hat{\mathbf{e}}_p$) are $\hat{\mathbf{e}}_{\pm} = (\hat{\mathbf{e}}_s \pm i\hat{\mathbf{e}}_p) / \sqrt{2}$.

We derive (as explained in detail in the discussion section) and analyze the spin-resolved emissivities $\eta_{(\pm)} = \eta(\omega, \theta, \phi, \hat{\mathbf{e}}_{\pm})$ and absorptivities $\alpha_{(\pm)} = \alpha(\omega, \theta, \phi, \hat{\mathbf{e}}_{\pm})$ defined above for planar configurations of several material classes. As a superset of materials, we consider a linear, time-invariant generic bianisotropic medium whose optical properties are described using the following

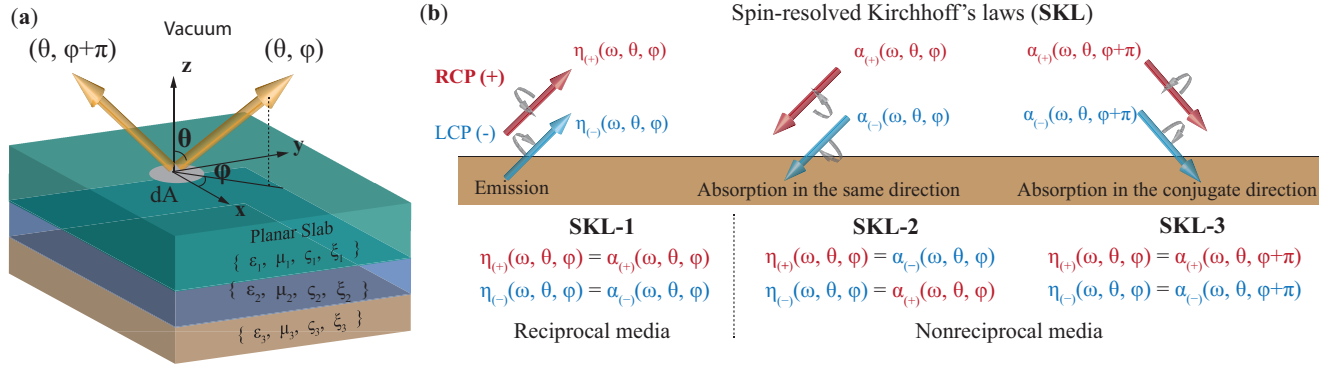


FIG. 1. (a) The figure shows the conventions used to describe the thermal radiation from the planar slab in a specific emission direction denoted by the angles (θ, ϕ) . Figure (b) summarizes the three spin-resolved Kirchhoff's laws that relate spin-resolved emissivities in (θ, ϕ) direction with spin-resolved absorptivities either along the same direction (θ, ϕ) or along the conjugate direction denoted by the angles $(\theta, \phi + \pi)$. The directions are consistently characterized based on the emission direction and not the absorption or wavevector directions. These laws are applicable for reciprocal and nonreciprocal materials presented in the table I and their multilayered or composite configurations as described in the main text.

No.	Material Class	Description	Examples	Kirchhoff's law
1	Reciprocal isotropic	$\bar{\epsilon}, \bar{\mu}$ are scalars, $\bar{\xi} = \bar{\zeta} = 0$	Common dielectric and metallic materials	SKL-1
2	Reciprocal anisotropic	Diagonal $\bar{\epsilon}$ with unequal entries, scalar $\bar{\mu}$, $\bar{\xi} = \bar{\zeta} = 0$.	Uniaxial and biaxial crystals [17]	SKL-1
3	Nonreciprocal gyroelectric	$\bar{\epsilon} \neq \bar{\epsilon}^T$, scalar $\bar{\mu}$, $\bar{\xi} = \bar{\zeta} = 0$.	Weyl semimetals [23], metals and semiconductors in magnetic field [20–22]	SKL-2,3
4	Nonreciprocal gyromagnetic	$\bar{\mu} \neq \bar{\mu}^T$, scalar $\bar{\epsilon}$, $\bar{\xi} = \bar{\zeta} = 0$.	Ferromagnets, ferrites [24]	SKL-2,3
5	Reciprocal magneto-electric	scalar $\bar{\epsilon}$ and $\bar{\mu}$, nonzero $\bar{\xi} = -\bar{\zeta}^T$.	Chiral media, metamaterials [18, 19]	SKL-1
6	Nonreciprocal magneto-electric	scalar $\bar{\epsilon}$ and $\bar{\mu}$, nonzero $\bar{\xi} = \bar{\zeta}^T$.	Topological insulator [26], Multi-ferroic media [25] and heterostructures [27]	SKL-2,3

TABLE I. Reciprocal and nonreciprocal material classes

constitutive relations in the frequency domain assuming local material response:

$$\mathbf{D} = \bar{\epsilon}\epsilon_0\mathbf{E} + \bar{\xi}\frac{1}{c}\mathbf{H}, \quad \mathbf{B} = \bar{\zeta}\frac{1}{c}\mathbf{E} + \bar{\mu}\mu_0\mathbf{H} \quad (3)$$

where $\bar{\epsilon}, \bar{\mu}$ are dimensionless permittivity and permeability tensors and $\bar{\xi}, \bar{\zeta}$ are magneto-electric coupling tensors. Such a material is reciprocal if these parameters satisfy the conditions $\bar{\epsilon} = \bar{\epsilon}^T, \bar{\mu} = \bar{\mu}^T, \bar{\xi} = -\bar{\zeta}^T$ where $(\dots)^T$ denotes the matrix transpose. It is nonreciprocal if any one of these conditions is violated. We consider a list of several material classes as shown in table I, which includes isotropic, uni/biaxial anisotropic, gyroelectric, gyromagnetic and magneto-electric materials. We discover that for multilayered or composite planar slabs of most of these material classes, the spin-resolved emissivities ($\eta_{(\pm)}$) and absorptivities ($\alpha_{(\pm)}$) satisfy specific relations described below and summarized in fig 1. They are called as spin-resolved Kirchhoff's laws (SKLs).

SKL-1: For multilayered or composite planar slabs of all reciprocal media, the spin-resolved emissivity in (θ, ϕ)

direction is equal to the spin-resolved absorptivity in *the same direction for each spin (polarization) state*.

$$\begin{aligned} \eta_{(+)}(\omega, \theta, \phi) &= \alpha_{(+)}(\omega, \theta, \phi) \\ \eta_{(-)}(\omega, \theta, \phi) &= \alpha_{(-)}(\omega, \theta, \phi) \end{aligned} \quad (4)$$

SKL-2: For multilayered or composite planar slabs of nonreciprocal media *that preserve the rotational symmetry in the plane of the surface* such as gyrotropic media with gyrotropy axis perpendicular to the surface and isotropic magneto-electric (Tellegen) media, the spin-resolved emissivity in (θ, ϕ) direction is equal to the spin-resolved absorptivity in *the same direction but of opposite spin state*.

$$\begin{aligned} \eta_{(+)}(\omega, \theta, \phi) &= \alpha_{(-)}(\omega, \theta, \phi) \\ \eta_{(-)}(\omega, \theta, \phi) &= \alpha_{(+)}(\omega, \theta, \phi) \end{aligned} \quad (5)$$

SKL-3: For multi-layered or composite planar slabs of nonreciprocal media *that do not preserve the rotational symmetry* in the plane of the surface such as gyrotropic media with gyrotropy axis parallel to the surface and anisotropic nonreciprocal magneto-electric media that cause cross coupling between perpendicular and parallel

components of $\mathbf{E} - \mathbf{H}$ fields ($E_x - H_z$, $E_z - H_x$, $E_y - H_z$, $E_z - H_y$), the spin-resolved emissivity in the direction (θ, ϕ) is equal to the spin-resolved absorptivity for the conjugate direction $(\theta, \phi + \pi)$ for each spin state.

$$\begin{aligned}\eta_{(+)}(\omega, \theta, \phi) &= \alpha_{(+)}(\omega, \theta, \phi + \pi) \\ \eta_{(-)}(\omega, \theta, \phi) &= \alpha_{(-)}(\omega, \theta, \phi + \pi)\end{aligned}\quad (6)$$

We emphasize that a multilayered or a composite planar slab which combines different material types following the same **SKL** also follows that same **SKL**. For instance, a planar slab which combines materials exhibiting gyrotropic and magnetoelectric response simultaneously, will follow **SKL-2** or **3** depending on the gyrotropy axis and the isotropic or anisotropic nature of the magnetoelectric response as described above. For conventional isotropic dielectric/metallic materials, all three laws hold since the spin-resolved emissivities and absorptivities are equal [$\eta_{(+)} = \eta_{(-)} = \alpha_{(+)} = \alpha_{(-)}$] in all relevant directions. It follows that a multilayered planar slab which contains layers of such trivial materials (satisfying all three **SKLs**) along with more exotic bianisotropic media satisfying a specific **SKL** can be readily described using that specific **SKL**. However, the laws are not applicable when the nontrivial bianisotropic media following distinct **SKLs** are combined. One example can be a planar slab containing layers of uniaxial anisotropic media (**SKL-1**) and gyrotropic media (**SKL-2** or **3**). Interestingly, we also find that a nonreciprocal magnetoelectric medium that leads to coupling between the parallel components of $\mathbf{E} - \mathbf{H}$ fields ($E_x - H_y$ or $E_y - H_x$) does not satisfy any one of these three **SKLs**. This special material is well-known in the literature for causing Fiegl effect and related phenomena [32–34]. Its uniqueness is related to the momentum asymmetry of light propagation inside this medium and it will be analyzed in more detail in our future work. Despite the few limiting cases, we note that **SKLs** are useful for thermal-radiation engineering using multi-layered or composite configurations of most bianisotropic materials, for all frequencies, emission directions, material and geometry parameters. In the following, we propose an experiment to verify these laws using a single material system.

B. Experimental proposal

We consider a doped Indium Antimonide (InSb) slab of thickness $t = 1\mu\text{m}$. and doping concentration $n = 10^{17}\text{cm}^{-3}$ (available at vendors like MTI Corp.) on top of a glass substrate of constant permittivity $\epsilon_s = 2.25$. We use the experimentally well-characterized Drude-Lorentz oscillator model [35–37] to calculate the permittivity of InSb with or without applied magnetic field [15]. In the absence of magnetic field, InSb slab

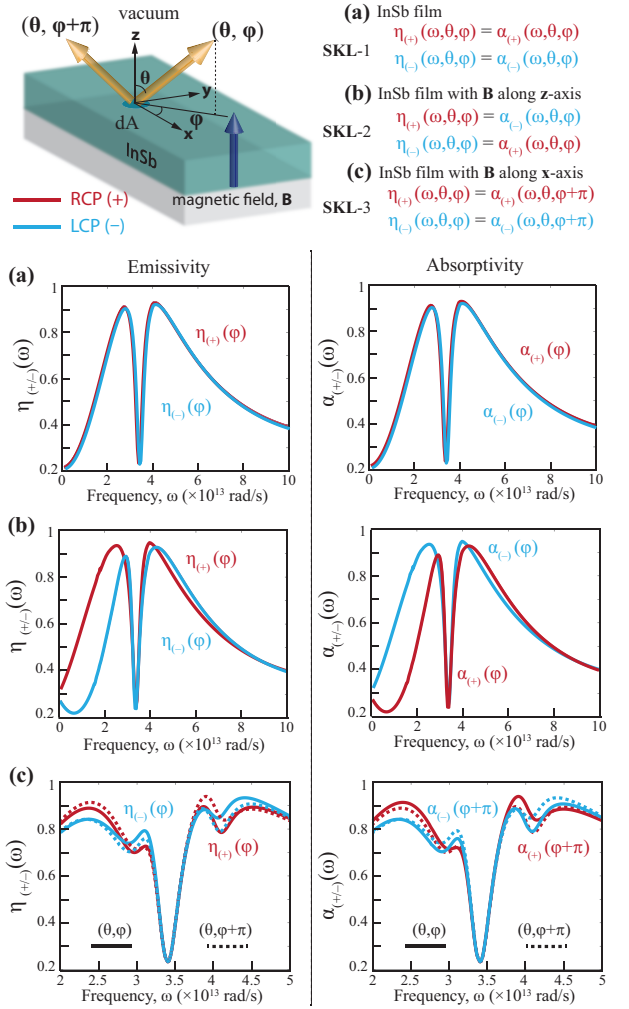


FIG. 2. The top schematic summarizes the three spin-resolved Kirchhoff's laws for a doped InSb slab with or without externally applied magnetic field. Figures (a,b,c) respectively demonstrate these laws. For brevity, we fix the direction as $(\theta = \pi/4, \phi = \pi/4)$. The first and second spin-resolved Kirchhoff's laws demonstrated in (a,b) respectively relate emissivities with absorptivities in the same direction. The third law demonstrated in (c) relates emissivity in a given direction with absorptivity in the conjugate direction $(\theta = \pi/4, \phi = \pi/4 + \pi)$.

has isotropic permittivity ($\bar{\epsilon}$) and permeability ($\bar{\mu}$), and $\bar{\xi}, \bar{\zeta} = 0$. Therefore, it is reciprocal in nature and follows **SKL-1**. In the presence of magnetic field, $\bar{\epsilon}$ has nonzero off-diagonal entries and InSb slab acts as a gyroelectric medium with the gyrotropy axis parallel to the applied field. Consequently, when the magnetic field is perpendicular or parallel to the surface, thermal radiation from InSb slab will follow either **SKL-2** or **SKL-3** respectively. In an experiment, the measurement of spin-resolved emissivities (Eq.9) and absorptivities (Eq.10) can be performed using a specific combination of polarizers and quarter-wave-plate optical components [5] in suitable directions of emission. Here, we calculate them as a function of frequency.

Figure 2 summarizes the three spin-resolved Kirchhoff's laws for the InSb slab (top schematic) and figures (a,b,c) demonstrate the calculated spectra of emissivities (left figures) and absorptivities (right figures). For brevity, we focus on the direction ($\theta = \pi/4, \phi = \pi/4$). As shown in Fig. 2(a), in the absence of magnetic field, the spin-resolved emissivities and absorptivities are equal for both spin states, RCP (red) and LCP (blue). The plots lie on top of each other. Figure 2(b) demonstrates **SKL-2**, where a magnetic field of strength 1T is applied perpendicular to the slab. Evidently, $\eta_{(+)} = \alpha_{(-)}$ and $\eta_{(-)} = \alpha_{(+)}$, which verifies **SKL-2**. Since $\eta_{(+)} \neq \eta_{(-)}$ in the given emission direction, the thermal emission from the slab will be partially spin-polarized. In Fig. 2(c), we consider a magnetic field of strength 2T applied along the \mathbf{x} -axis of the geometry. This example demonstrates that spin-resolved emissivities in (θ, ϕ) direction are equal to spin-resolved absorptivities for the same spin state but in the conjugate $(\theta, \phi + \pi)$ direction. Thus, **SKL-3** can be verified.

C. Universal perspective of spin-resolved thermal emission

In the context of spin-resolved thermal radiation, it is illuminating to answer two fundamental questions. First, what materials can emit spin-polarized or circularly polarized thermal radiation? And second, what materials can experience nontrivial torque and force upon thermal emission of spin-polarized photons? We answer both these questions with a universal perspective of all material classes listed in the table I. Note that we consider nonequilibrium situation unlike equilibrium thermal radiation for derivation of **SKLs**. We focus on thermal emission from the planar slab at temperature T_0 into the surrounding vacuum at $T = 0\text{K}$. The strength of the circular polarization of thermal emission is characterized using the well-known experimentally accessible Stokes S_3 parameter defined as:

$$S_3(\omega, \theta, \phi) = \frac{\eta_{(+)}(\omega, \theta, \phi) - \eta_{(-)}(\omega, \theta, \phi)}{\eta_{(+)}(\omega, \theta, \phi) + \eta_{(-)}(\omega, \theta, \phi)} \quad (7)$$

$S_3 = +1$ denotes pure RCP light while $S_3 = -1$ denotes pure LCP light in the given emission direction. When the planar slab emits thermal radiation into the environment at lower temperature, it loses linear and angular momentum carried away by the photons, and consequently experiences force and torque respectively. We compute the spectral force per unit area (\mathbf{F}_s given by Eq. 18) and the spectral torque per unit area ($\boldsymbol{\tau}_s$ given by Eq. 19) experienced by the planar slab due to the emission of photons of frequency ω by integrating over all emission directions. The derivation of these quantities is provided in section III.

Figure 3 summarizes all materials that can emit partially spin-polarized thermal radiation in suitable directions. For illustration, we consider a planar slab of a material characterized by $\bar{\epsilon}, \bar{\mu}, \bar{\xi}, \bar{\zeta}$ at a temperature T_0 emitting into the surrounding vacuum at $T = 0\text{K}$. Similar to our previous work [15], we provide a universal perspective by analyzing the representative examples of several material classes using reasonable values of the material parameters evaluated at a frequency ω and importantly, satisfying the thermodynamic passivity constraint [38]. While the constitutive relations in Eq. 3 can, in principle, be used to describe optically active gain media, our radiometry analysis is applicable for passive media based on the detailed balance at thermal equilibrium. Hence, passivity of the medium must be ensured [15]. We assume the thickness of the planar slab to be $d = 0.5c/\omega$. The contour plot for each representative example demonstrates the variation of the Stokes S_3 parameter as a function of the emission direction characterized by (θ, ϕ) in spherical coordinates. The calculated spectral force and torque per unit area provided for each example reveal the zero or nonzero values and the directions of these quantities for all materials belonging to that particular class. While there are many new interesting results in this figure, a detailed discussion involving frequency-dependent response of real materials of each type is beyond the scope of the present work. Nonetheless, this universal perspective is useful because we can provide a signature of new interesting possibilities which can then be explored in more detail in the future.

Circularly polarized thermal emission: First, we note a surprising result that there are many materials whose planar slabs can emit partially spin-polarized thermal radiation. This is evident from the nonzero values of S_3 parameters demonstrated using contour plots in Fig.3 for several material classes. This includes all nonreciprocal planar media and also reciprocal media like uni/bi-axial anisotropic materials and reciprocal magnetoelectric (chiral) media. For uni-axial anisotropic media, we assume anisotropy to be in the plane of the slab surface (\mathbf{xy} -plane). Note that all materials belonging to these material classes except artificial metamaterials do not require any surface patterning or geometric chirality which is essential for observing circularly polarized thermal radiation in previous experiments [4, 5]. Another result is the subtle difference between spin-resolved emission from gyrotropic media and that from nonreciprocal magnetoelectric media. Particularly, gyrotropic media with gyrotropy axis perpendicular to surface (examples 3,4,7) and nonreciprocal isotropic magnetoelectric (Tellegen) media (example 13) both satisfy **SKL-2** as discussed above. However, for magnetoelectric media, the spin-resolved emission is symmetric with respect to top ($\theta \in [0, \pi/2)$) and bottom hemispheres ($\theta \in [\pi/2, \pi]$) whereas it is asymmetric for

Universal perspective of thermal spin photonics for thin films of reciprocal and nonreciprocal materials

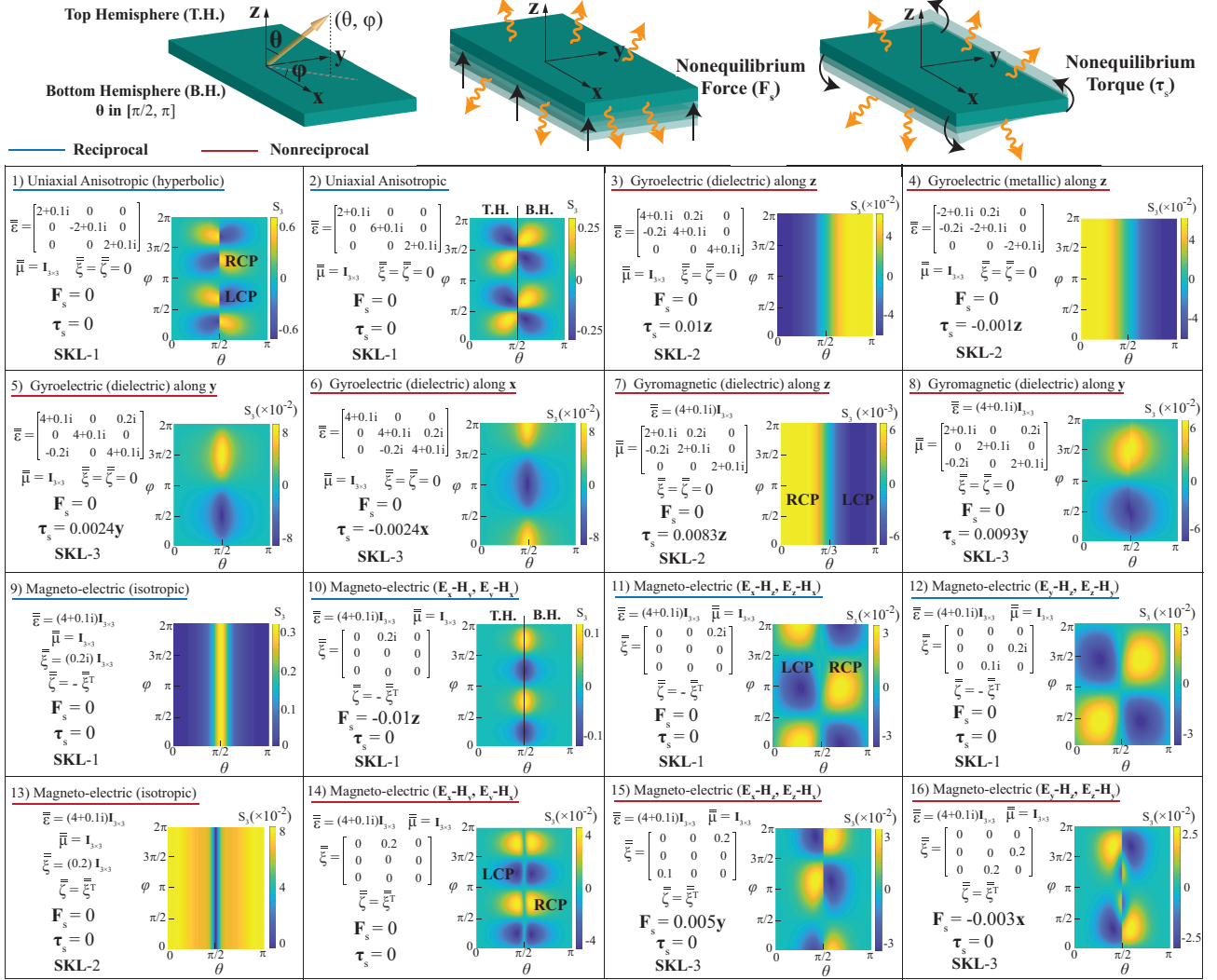


FIG. 3. This figure analyzes circularly polarized thermal emission and associated nonequilibrium force and torque for several material classes using representative examples. We consider thermal emission at frequency ω from a planar slab of thickness $d = 0.5c/\omega$ at temperature T_0 into the surrounding vacuum on both sides at temperature $T = 0\text{K}$. The contour plot in each representative example demonstrates the Stokes S_3 parameter (Eq.7) as a function of (θ, ϕ) which are given in the top left inset. The calculated spectral force per unit area $\mathbf{F}_s/(I_b T_0/2c)$ and spectral torque per unit area $\boldsymbol{\tau}_s/(I_b T_0/2\omega)$ arising from the thermal emission from the slab are provided for given material parameters. The applicable spin-resolved Kirchhoff's law (SKL) is also noted for each example.

gyrotropic media. The asymmetry can be predicted based on the microscopic picture of underlying cyclotron motion. If the thermally or statistically averaged cyclotron motion of electrons is anti-clockwise in the xy -plane (perpendicular gyrotropy axis) as viewed from $+z$ -direction, the resulting emission should be RCP along $+z$ -direction and LCP along $-z$ -direction.

We also point out that the material classes lead to unique dependence of S_3 on the emission directions which is evident from the contour plots. This can be informative from the perspective of classifying or identifying materials using infrared imaging polarimetry in an actual experiment.

Nonequilibrium torque: We find that all gyrotropic

planar slabs experience a net nonzero torque along the direction of the gyrotropy axis (examples 3 to 8) because of the overall loss of angular momentum via emission of spin-polarized photons. For isotropic magneto-electric (Tellegen and Pasteur) media (examples 9,13), the total spectral torque per unit area is zero which follows from the symmetry in top and bottom hemispheres discussed above. For other materials, the net torque is zero because of the cancellation upon integration over the angle ϕ . Note that we have focused on the planar slabs of individual material classes for illustration.

For multilayered configurations combining different material classes, a net nonzero torque can be obtained along a specific direction even though it is absent for

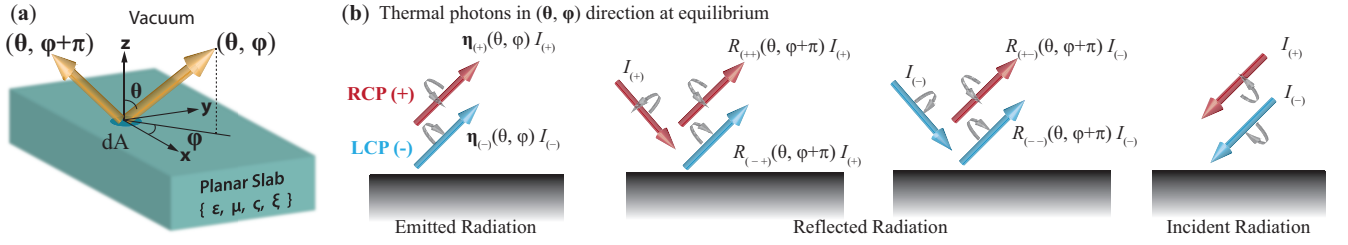


FIG. 4. (a) The figure demonstrates the conventions used to describe the thermal radiation from the planar surface in a specific direction. The angles (θ, ϕ) characterize the emission direction (not the direction of incidence). Figure (b) illustrates the spectral radiance of thermal photons in (θ, ϕ) direction when the planar slab is at thermal equilibrium with the surrounding vacuum. These energy flux rates are described using the spin-resolved blackbody radiance (I_{\pm}), emissivities (η_{\pm}) and interconversion reflectances (R) for radiation incident along the conjugate $(\theta, \phi + \pi)$ direction.

a single-layered slab. For instance, if the isotropic magnetoelectric medium (examples 9, 13) is deposited on top of another thin film of common dielectric or metallic material, a net nonzero torque along z -axis can be obtained because of the asymmetric overall emission of spin-polarized photons in top and bottom hemispheres. We provide these results for multilayered slabs in the supplement. Based on a universal perspective, we identify material classes required for engineering perpendicular and parallel components of the nonequilibrium torque. We find that only materials satisfying **SKL-2** (examples 3,4,7,13) and isotropic reciprocal magnetoelectric (Pasteur) media (example 9) can experience *perpendicular* nonequilibrium torque in a multilayered configuration. Only materials satisfying **SKL-3** (examples 5,6,8,15,16) and anisotropic reciprocal magnetoelectric media (examples 11,12) can experience *parallel* nonequilibrium torque in a multilayered configuration.

Nonequilibrium force: Figure 3 reveals that for a single-layered geometry, only a reciprocal magnetoelectric planar slab that causes cross coupling between $E_x - H_y$ and $E_y - H_x$ fields (example 10), can lead to a nonzero nonequilibrium force along z -axis. For other materials, the symmetry of overall thermal emission (summed over both spin states) in top and bottom hemispheres leads to cancellation of the resulting force along z -axis. The figure also reveals that only planar slabs of anisotropic nonreciprocal magnetoelectric materials (examples 15,16) can experience nonequilibrium force parallel to the surface whose direction is determined by the nature of the magneto-electric coupling. If the magnetoelectric tensors $(\bar{\xi}, \bar{\zeta})$ indicate $(E_x - H_z, E_z - H_x)$ -type cross coupling, the net force is along y -axis. If they indicate $(E_y - H_z, E_z - H_y)$ -type cross coupling, this force is along x -axis. The multilayered slabs of other material classes can also lead to nonequilibrium force as discussed in the supplement. Based on a universal perspective, we find that all material classes can experience a *perpendicular* nonequilibrium force in a

multilayered configuration and only materials satisfying **SKL-3** can experience a *parallel* nonequilibrium force in a multilayered configuration. These results indicate the possibility of engineering thermal-nonequilibrium optomechanical forces and torques in planar geometries and identifying or classifying materials based on experimentally measurable characteristics.

III. DISCUSSION

A. Spin-resolved emissivities and absorptivities

First, we derive the spin-resolved emissivities and absorptivities for a semi-infinite half-space because of its simplicity and connection with the fluctuational electrodynamic theory as explained in the supplement. We then extend the derivation for a finite-thickness planar slab. Since we assume linear material response and regular reflection from the surface, the frequency ω and the angle θ are not changed upon reflection. Hence, we can apply the principle of total energy conservation for energy-exchange channels characterized by ω, θ separately and focus on the polarization or spin-dependent properties. The flux rates are given by equations 1 and 2.

Figure 4(b) depicts the spin-resolved energy flux rates (RCP and LCP radiation) at frequency ω in the direction (θ, ϕ) which contain emitted, reflected and incident radiation. The fluxes are described at thermal equilibrium within the radiometry paradigm [39]. As shown in the rightmost figure, the incident radiation contains both RCP ($I_{(+)}$) and LCP ($I_{(-)}$) radiation. Since the incident blackbody radiation is unpolarized, it follows that $I_{(+)} = I_{(-)} = I_b/2$. The emitted radiation is described using the spin-resolved emissivities as $\eta_{(+)}I_{(+)}$ (RCP) and $\eta_{(-)}I_{(-)}$ (LCP). The reflected radiation arises from the radiation incident along the conjugate direction $(\theta, \phi + \pi)$ and is described using the polarization interconversion reflectances. For instance, as shown in the second figure in 4(b), the incident RCP radiation

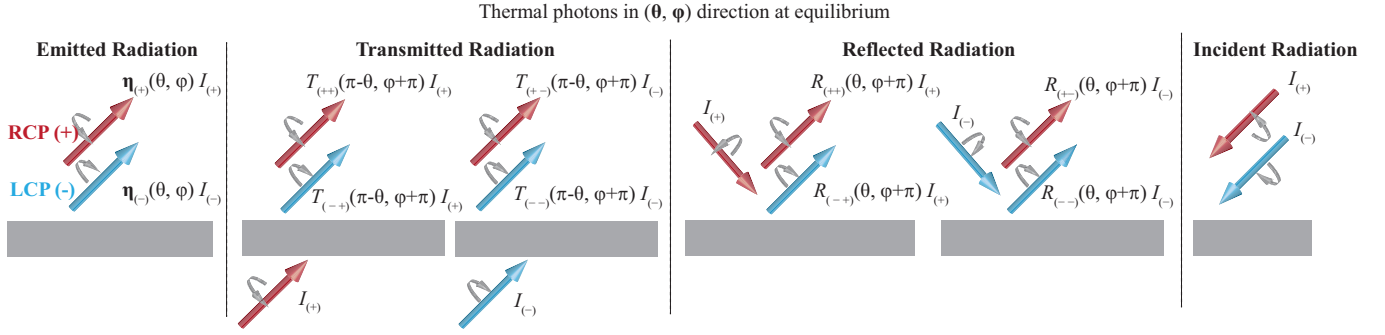


FIG. 5. This figure illustrates the spectral radiance of thermal photons in (θ, ϕ) direction when the finite-thickness planar slab is at thermal equilibrium with the surrounding vacuum on both sides. These energy flux rates are described using the spin-resolved blackbody radiance (I_{\pm}), emissivities (η_{\pm}) and interconversion reflectances and transmittances. The emissivities are obtained by the equality of spin-resolved flux rates in opposite directions in the far-field under thermal equilibrium condition.

($I_{(+)}$) gets reflected as $R_{(++)}(\theta, \phi + \pi)I_{(+)}$ (RCP) and $R_{(-+)}(\theta, \phi + \pi)I_{(+)}$ (LCP) along (θ, ϕ) direction. Note that we have characterized directions based on the emitted radiation (indicated by arrows in (a)) and not the incident radiation. This avoids the ambiguity in characterizing directions for a thin film (finite-thickness slab described below) where transmitted radiation is also taken into account. The interconversion reflectances can be measured separately in an experiment or can be calculated for the planar slab using the well-known Fresnel reflection coefficients ($r_{ss}, r_{sp}, r_{ps}, r_{pp}$) using the following expressions (omitting the dependence on θ, ϕ for brevity):

$$\begin{aligned} R_{(++)/--} &= |(r_{ss} + r_{pp}) \pm i(r_{sp} - r_{ps})|^2/4 \\ R_{(-+)/(+-)} &= |(r_{ss} - r_{pp}) \pm i(r_{sp} + r_{ps})|^2/4 \end{aligned} \quad (8)$$

The Fresnel reflection coefficient r_{jk} for $j, k = [s, p]$ denotes the amplitude of j-polarized reflected wave due to unit amplitude k-polarized incident wave. Since the overall radiation in the far-field is isotropic and unpolarized at thermal equilibrium, the spin-resolved energy flux rates in opposite directions are equal. This argument is justified by our previous work [15] which shows that the equilibrium spin angular momentum density and the Poynting flux of thermal radiation are always zero in the far-field although they can be nonzero in the near-field of certain nonreciprocal media. By equating the incoming and outgoing spin-resolved radiation flux rates in the far-field, we obtain the following spin-resolved emissivities in terms of reflectances:

$$\begin{aligned} \eta_{(+)}(\theta, \phi) &= 1 - R_{(++)}(\theta, \phi + \pi) - R_{(-+)}(\theta, \phi + \pi) \\ \eta_{(-)}(\theta, \phi) &= 1 - R_{(--)}(\theta, \phi + \pi) - R_{(+)}(\theta, \phi + \pi) \end{aligned} \quad (9)$$

Similarly, it is straightforward to obtain the spin-resolved absorptivities by considering the reflection of incident polarized radiation $I_{(\pm)}$ separately. By subtracting the reflected flux from the incident radiation

flux, we obtain the following spin-resolved absorptivities:

$$\begin{aligned} \alpha_{(+)}(\theta, \phi) &= 1 - R_{(++)}(\theta, \phi) - R_{(-+)}(\theta, \phi) \\ \alpha_{(-)}(\theta, \phi) &= 1 - R_{(--)}(\theta, \phi) - R_{(+)}(\theta, \phi) \end{aligned} \quad (10)$$

We show in the supplement that the emissivities (Eq.9) can be obtained within the scattering matrix formulation of fluctuational electrodynamics theory. We further validate this derivation by proving the thermodynamic consistency condition of net zero exchange of linear and angular momentum of the planar slab with the environment at thermal equilibrium. But before that, we extend this analysis to obtain the spin-resolved emissivities and absorptivities for a planar slab of finite thickness.

For a finite-thickness slab surrounded by vacuum on both sides, the incident radiation, in addition to getting reflected, also gets transmitted to the other side of the slab. It is straightforward to obtain the emissivities in terms of reflectances and transmittances using similar energy-balance considerations. In particular, as shown in Fig.5, the radiation in the direction (θ, ϕ) contains emitted, transmitted, reflected and incident photons. The transmitted radiation in (θ, ϕ) direction arises from the radiation incident in the direction $(\pi - \theta, \phi + \pi)$ on the other side as depicted in Fig.5(b). The directions are consistently characterized based on the emission directions and not the directions of the incidence or the associated wavevectors. The transmittances are calculated from the associated Fresnel transmission coefficients ($t_{ss}, t_{sp}, t_{ps}, t_{pp}$) using the expressions (omitting the dependence on θ, ϕ for brevity):

$$\begin{aligned} T_{(++)/--} &= \frac{1}{4} |(t_{ss} + t_{pp}) \pm i(t_{sp} - t_{ps})|^2 \\ T_{(-+)/(+-)} &= \frac{1}{4} |(t_{ss} - t_{pp}) \pm i(t_{sp} + t_{ps})|^2 \end{aligned} \quad (11)$$

The transmission coefficient t_{jk} for $j, k = [s, p]$ denotes the amplitude of j-polarized transmitted wave due to unit amplitude k-polarized incident wave. Equating outgoing

and incoming spin-resolved flux rates in the opposite directions in the far-field, we obtain the following expressions for the spin-resolved emissivities:

$$\begin{aligned}\eta_{(+)}(\theta, \phi) &= 1 - R_{(+)}(\theta, \phi + \pi) - R_{(++)}(\theta, \phi + \pi) \\ &\quad - T_{(+)}(\pi - \theta, \phi + \pi) - T_{(++)}(\pi - \theta, \phi + \pi) \\ \eta_{(-)}(\theta, \phi) &= 1 - R_{(-)}(\theta, \phi + \pi) - R_{(--)}(\theta, \phi + \pi) \\ &\quad - T_{(-)}(\pi - \theta, \phi + \pi) - T_{(--)}(\pi - \theta, \phi + \pi)\end{aligned}\quad (12)$$

Similarly, the spin-resolved absorptivities are obtained by subtracting the reflected and transmitted flux rates from the incident polarized flux rates.

$$\begin{aligned}\alpha_{(+)}(\theta, \phi) &= 1 - R_{(+)}(\theta, \phi) - R_{(++)}(\theta, \phi) \\ &\quad - T_{(+)}(\theta, \phi) - T_{(++)}(\theta, \phi) \\ \alpha_{(-)}(\theta, \phi) &= 1 - R_{(-)}(\theta, \phi) - R_{(--)}(\theta, \phi) \\ &\quad - T_{(-)}(\theta, \phi) - T_{(--)}(\theta, \phi)\end{aligned}\quad (13)$$

Detailed balance of linear and angular momentum exchange: We now demonstrate the theoretical consistency of the above derivation by showing detailed balance of linear and angular momentum exchange between the slab and its surroundings which must be maintained at thermal equilibrium. Since angular momentum remains a largely unexplored topic in the field of thermal radiation [29, 40], we explain it in detail. A circularly polarized plane wave in vacuum normalized to describe a single photon carries linear momentum of $\hbar\omega/c$ and angular momentum of $\pm\hbar$ along its direction of propagation. It carries only spin angular momentum since the orbital contributions are zero. Intrinsic orbital angular momentum is zero because of the plane wavefront and extrinsic orbital angular momentum is zero because of the cancellation over its infinite transverse extent [41, 42]. It also follows from the spin angular momentum density expression [$\sim \text{Im}\{\mathbf{E}^*(\omega) \times \mathbf{E}(\omega)\}$] that there are no cross-polarization interaction terms in the net angular momentum when the radiation consists of both RCP ($\hat{\mathbf{e}}_{(+)}$) and LCP ($\hat{\mathbf{e}}_{(-)}$) photons. Therefore, similar to the energy flux, the angular momentum flux of thermal photons can be considered separately for both polarization states. Calculating the photon number flux rates using Eqs. 1 and 2, we obtain both linear and angular momentum flux rates for a finite-thickness planar slab. The rates for a semi-infinite half-space are obtained by choosing zero transmittances.

The rate of change of linear momentum $d\mathbf{p}/dt$ along $+\mathbf{z}$ -direction of the planar slab due to absorption, reflection, and transmission of photons incident along (θ, ϕ) direction and emitted by the slab along the same direction is given below (abbreviating $dM =$

$|\cos\theta|d\omega d\Omega dA$ in Eq.1 for simplicity):

$$\begin{aligned}\frac{dp_z}{dt}(\theta, \phi) &= \left[\overbrace{-(\alpha_{(+)} + \alpha_{(-)})I_b(T_{\text{env}})}^{\text{absorption}} - \overbrace{(\eta_{(+)} + \eta_{(-)})I_b(T_0)}^{\text{emission}} \right. \\ &\quad \left. + \sum_{j,k=(+,-)} \overbrace{-2R_{(jk)}I_b(T_{\text{env}})}^{\text{reflection}} \right] \frac{1}{2c} \cos\theta dM\end{aligned}\quad (14)$$

where T_0 is the temperature of the slab and T_{env} is the temperature of the environment. The dependence of various quantities on (ω, θ, ϕ) is assumed and not mentioned above for brevity. As an explanation of various terms, we consider incident RCP (+) radiation in the top hemisphere and find the linear momentum change of the slab along $+\mathbf{z}$ -axis. It follows that $\alpha_{(+)}$ portion gets absorbed imparting momentum $\propto -\cos\theta\alpha_{+}I_{b,T_{\text{env}}}\hbar\omega/c$, $R_{(++)} + R_{(-)}$ portion gets reflected in the positive \mathbf{z} -direction imparting momentum $\propto -2\cos\theta(R_{(++)} + R_{(-)})I_{b,T_{\text{env}}}\hbar\omega/c$, and $T_{(++)} + T_{(-)}$ portion gets transmitted to the bottom hemisphere without imparting any momentum to the slab. Because of the emission of RCP radiation in the same direction, momentum $\propto -\cos\theta\eta_{(+)}I_{b,T_0}$ is imparted to the slab. Negative sign corresponds to the loss of the linear momentum by the slab.

Similarly, we obtain the rate of change of angular momentum ($d\mathbf{J}/dt$) of the planar slab whose \mathbf{z} -component is:

$$\begin{aligned}\frac{dJ_z}{dt}(\theta, \phi) &= \left[\overbrace{-(\alpha_{(+)} - \alpha_{(-)})I_{b,T_{\text{env}}}}^{\text{absorption}} - \overbrace{(\eta_{(+)} - \eta_{(-)})I_{b,T_0}}^{\text{emission}} \right. \\ &\quad \left. - 2\overbrace{(R_{(++)} - R_{(--)} + T_{(-)} - T_{(++)})I_{b,T_{\text{env}}}}^{\substack{\text{reflection} \\ \text{transmission}}} \right] \frac{1}{2\omega} \cos\theta dM\end{aligned}\quad (15)$$

The \mathbf{x} -components of both linear and angular momentum transfer rates are:

$$\begin{aligned}\frac{dp_x}{dt}(\theta, \phi) &= \left[-(\alpha_{(+)} + \alpha_{(-)})I_{b,T_{\text{env}}} \right. \\ &\quad \left. - (\eta_{(+)} + \eta_{(-)})I_{b,T_0} \right] \frac{1}{2c} \sin\theta \cos\phi dM\quad (16) \\ \frac{dJ_x}{dt}(\theta, \phi) &= \left[-(\alpha_{(+)} - \alpha_{(-)})I_{b,T_{\text{env}}} - (\eta_{(+)} - \eta_{(-)})I_{b,T_0} \right. \\ &\quad \left. - 2(R_{(-)} - R_{(++)} + T_{(-)} - T_{(++)})I_{b,T_{\text{env}}} \right] \frac{\sin\theta \cos\phi dM}{2\omega}\end{aligned}\quad (17)$$

The \mathbf{y} -components are obtained by replacing $\cos\phi$ with $\sin\phi$ in above two expressions. It is then straightforward to calculate the spectral force per unit area (\mathbf{F}_s) and the spectral torque per unit area ($\boldsymbol{\tau}_s$) experienced by the planar slab due to the thermal emission of photons of

frequency ω :

$$\mathbf{F}_s = \frac{d\mathbf{F}}{d\omega dA}(\omega) = \int \frac{d\mathbf{p}}{dt d\omega dA}(\omega, \theta, \phi) \quad (18)$$

$$\boldsymbol{\tau}_s = \frac{d\boldsymbol{\tau}_s}{d\omega dA}(\omega) = \int \frac{d\mathbf{J}}{dt d\omega dA}(\omega, \theta, \phi) \quad (19)$$

Here the integration is over the solid angle $d\Omega$ and the terms in the denominator $d\omega dA$ come from dM introduced in Eqs 14,15,16,17. The final expressions are integrated over the frequency ω for calculating total force and total torque per unit area.

We now substitute the spin-resolved emissivities (Eq.12) and absorptivities (Eq.13) in the above expressions and compute the rates of linear and angular momentum transfer under thermal equilibrium condition ($T_0 = T_{\text{env}}$). We find that the following vectorial equalities always hold true:

$$\begin{aligned} \frac{d\mathbf{p}}{dt}(\theta, \phi) + \frac{d\mathbf{p}}{dt}(\theta, \phi + \pi) \\ + \frac{d\mathbf{p}}{dt}(\pi - \theta, \phi) + \frac{d\mathbf{p}}{dt}(\pi - \theta, \phi + \pi) = 0 \\ \frac{d\mathbf{J}}{dt}(\theta, \phi) + \frac{d\mathbf{J}}{dt}(\theta, \phi + \pi) \\ + \frac{d\mathbf{J}}{dt}(\pi - \theta, \phi) + \frac{d\mathbf{J}}{dt}(\pi - \theta, \phi + \pi) = 0 \quad (20) \end{aligned}$$

It follows upon integration over all emission directions that there is no net force or torque on the planar slab which is at thermal equilibrium with the surrounding environment. Since the spin-resolved emissivities (Eq.12) are derived without invoking the concept of electromagnetic reciprocity, and are new to the best of our knowledge, we note that the above analysis of detailed balance of linear and angular momentum transfer provides a thermodynamic consistency of the derivation. The above derivation is also crucial for computing the fluctuations-induced force and torque on the planar slabs under the nonequilibrium condition when $T_{\text{env}} \neq T_0$ as discussed above.

B. Derivation of Spin-resolved Kirchhoff's laws

The calculation of spin-resolved emissivities and absorptivities requires the calculation of Fresnel reflection and transmission coefficients. While this is a very well-known topic in the literature, we note that, apart from the trivial isotropic media, the closed-form semi-analytic expressions of reflection coefficients are possible only for semi-infinite half-spaces of very few bianisotropic material classes [43–45]. We separately show this calculation in the supplement for a gyromagnetic medium. However, the semi-analytic approach is inadequate because we are interested in finding the laws which are applicable for a generic case of

a finite-thickness slab that can possibly contain multiple layers of various materials. It can also be a composite medium where a single layer can simultaneously exhibit response of multiple material classes. Since meaningful closed-form expressions are not possible for these complicated cases, we have developed numerical tools to calculate the reflection and transmission coefficients in an exact manner as discussed in the methods section. We have made them open-source[46] so that the reader can reproduce and verify the results in this work and also use these versatile tools for any other research activities. Our computer-assisted but exact approach for the discovery of Kirchhoff's laws is similar in spirit to that of an increasing use of machine learning, optimization, and inverse design computational techniques in many scientific disciplines for making fundamental discoveries.

Reciprocal materials: For a planar slab of reciprocal media, we find that the reflection coefficients satisfy the relations $r_{ss,pp}(\theta, \phi) = r_{ss,pp}(\theta, \phi + \pi)$ and $r_{sp}(\theta, \phi) = -r_{ps}(\theta, \phi + \pi)$. The transmission coefficients satisfy $t_{ss,pp}(\theta, \phi) = t_{ss,pp}(\pi - \theta, \phi + \pi)$ and $t_{sp}(\theta, \phi) = -t_{ps}(\pi - \theta, \phi + \pi)$. These relations can be inferred from the Green's function on the vacuum side of the geometry [47]. Substituting these relations in Eqs. 12 and 13, we find that the spin-resolved emissivity is equal to the spin-resolved absorptivity for reciprocal media. $\eta_{\pm}(\omega, \theta, \phi) = \alpha_{\pm}(\omega, \theta, \phi)$. This is **SKL-1** given in Eq. 4. For a chiral absorber $\alpha_{(+)} \neq \alpha_{(-)}$ from which it follows that $\eta_{(+)} \neq \eta_{(-)}$. Therefore, a chiral absorber can emit circularly polarized thermal radiation. But this well-known law is valid only for reciprocal media. Interestingly, for nonreciprocal media, we find other formulations of this spin-resolved Kirchhoff's law.

Nonreciprocal materials: For gyrotropic materials with the gyrotropy axis perpendicular to the planar surface and for nonreciprocal isotropic magneto-electric materials (Tellegen media) having diagonal $\bar{\bar{\xi}}, \bar{\bar{\zeta}}$ tensors, we find that the reflection coefficients satisfy the relations $r_{ss,pp}(\theta, \phi) = r_{ss,pp}(\theta, \phi + \pi)$ and $r_{sp}(\theta, \phi) = r_{ps}(\theta, \phi + \pi)$. The transmission coefficients satisfy the relations $t_{ss,pp}(\theta, \phi) = t_{ss,pp}(\pi - \theta, \phi + \pi)$ and $t_{sp}(\theta, \phi) = t_{ps}(\pi - \theta, \phi + \pi)$. Substituting these relations in Eqs. 12 and 13, we obtain $\eta_{\pm}(\omega, \theta, \phi) = \alpha_{\mp}(\omega, \theta, \phi)$. This is **SKL-2** given in Eq. 5.

Interestingly, multilayered planar slabs of other nonreciprocal gyrotropic and anisotropic magneto-electric materials also exhibit simplifying relations between the Fresnel coefficients. In particular, if the magnetoelectric coupling tensors $(\bar{\bar{\xi}}, \bar{\bar{\zeta}})$ indicate cross coupling between electric and magnetic fields lying perpendicular and parallel to the slab ($E_x - H_z, E_z - H_x, E_y - H_z$ or $E_z - H_y$) or if the medium is gyrotropic with the gyrotropy axis parallel to the surface, the reflection coefficients satisfy the condition $r_{sp}(\theta, \phi) = -r_{ps}(\theta, \phi)$ and the transmission coefficients satisfy $t_{ss,pp}(\pi - \theta, \phi +$

$\pi) = t_{ss,pp}(\theta, \phi + \pi)$ and $t_{sp}(\pi - \theta, \phi + \pi) = -t_{ps}(\theta, \phi + \pi)$. Substituting these relations in Eqs. 12 and 13, we obtain $\eta_{\pm}(\omega, \theta, \phi) = \alpha_{\pm}(\omega, \theta, \phi + \pi)$. This is **SKL-3** given in Eq. 6. We note that the above underlying relations are not obvious and their universal applicability for multilayered or composite configurations of many bianisotropic material classes has not been reported before. The explanation of their specific form based on the underlying structural characteristics or symmetries of material classes is a nontrivial problem that motivates new analogies or methods [48] across a broad set of materials.

IV. CONCLUDING REMARKS

We consider a different perspective of spin-resolved or spin-polarized thermal radiation and analyze it comprehensively for reciprocal and nonreciprocal media. We use radiometry paradigm to derive the spin-resolved emissivity and absorptivity without invoking the concept of electromagnetic reciprocity. We further provide a validation of this derivation by showing the detailed balance of both linear and angular momentum transfer rates when the planar slab is at thermal equilibrium with its environment. The spin-resolved expressions ensure that there is no net nonzero force or torque on the planar slab which is a necessary condition to maintain thermal equilibrium with the environment. Our emphasis on these theory details and derivation is important because, although thermal radiation is a very old topic, its extension to nonreciprocal media is a recent development and reviving the old radiometry paradigm in that context (uncommon in recent works) requires careful analysis. Besides, the concept of detailed balance of angular momentum (in addition to energy) provides a fundamentally new insight related to the interplay of photon spin and thermal radiation. This concept can be extended to analyze heat transfer at thermal equilibrium in many other systems for validating underlying physical models or deriving similar heat-transfer laws.

Through a universal perspective of spin-resolved thermal emission for generic bianisotropic material classes, we discover three useful spin-resolved Kirchhoff's laws of thermal radiation applicable for reciprocal and nonreciprocal planar media. While the first law applicable for the reciprocal media (**SKL-1**) is known, the remaining two laws for the nonreciprocal planar media are new. We emphasize that these laws are applicable for composite media or multilayered configurations of many material classes, for all frequencies, emission directions, geometry and material parameters. Since Kirchhoff's laws are at the foundation of the field of thermal radiation and are applicable only for reciprocal media, their generalization to nonreciprocal media is a very important fundamental result.

We also propose an experiment to verify the spin-resolved Kirchhoff's laws conveniently by using a single material system. We note that we can obtain another formulation of directional Kirchhoff's laws relating total emissivity ($\eta = \eta_{(+)} + \eta_{(-)}$) with total absorptivity ($\alpha = \alpha_{(+)} + \alpha_{(-)}$) by summing over both spin polarization states. The spin-resolved Kirchhoff's laws and their derivatives will be useful for optimizing directional radiative heat transfer [7, 28] and engineering broadband circularly polarized thermal emission [5].

While the calculation of Fresnel coefficients for specific cases of bianisotropic media is a well-known topic in the literature, a universal perspective revealing the interesting underlying relations in this work is new to the best of our knowledge in that research area. They can be potentially used for discovering similar laws concerning different (not necessarily thermal) radiation properties. Moreover, we emphasize that this work is not merely the derivation of Fresnel coefficients. The central results are not obvious from the existing literature on Fresnel coefficients for bianisotropic media, since they primarily depend on the important theory details and derivation provided in this work. We also note that the concepts like spin-resolved radiative heat transfer, bianisotropic media, photon spin and angular momentum remain largely unexplored in the field of thermal radiation (see recent reviews [49]). Our work simultaneously advances these new frontiers. We believe that these inquiries will be insightful for other research areas. For example, angular momentum transfer via spin-polarized thermal radiation (a different perspective introduced here and in our previous work [15]) can be relevant in the separate field of spintronics.

In addition to the spin-resolved Kirchhoff's laws, we also show other thermal spin photonic features for several material classes. First, we show a striking result that the planar media of many materials can emit spin-polarized thermal light. This includes all nonreciprocal media as well as reciprocal media such as uni/bi-axial anisotropic crystals and reciprocal magnetoelectric (chiral) media. Second, we demonstrate nonequilibrium force and torque experienced by planar slabs due to the loss of linear and angular momentum respectively, via thermal radiation into the environment at lower temperature. We also identify the material classes that can be used for engineering parallel and perpendicular components of nonequilibrium force and torque in multilayered planar slabs. These findings will be useful from the perspective of practical applications such as designing directional and spin-polarized light sources, engineering thermal optomechanical forces and torques, and classifying or identifying materials using infrared imaging polarimetry.

V. METHODS

The calculation of Fresnel reflection and transmission coefficients for the planar media involves two steps. The first step requires calculation of the wavevectors and the plane-wave solutions of the electromagnetic fields inside each layer of the planar slab. We consider most general multi-layered geometry. The second step involves the calculation of these coefficients by enforcing the boundary conditions at each interface for incidence of either $\hat{\mathbf{e}}_s$ or $\hat{\mathbf{e}}_p$ polarized light.

A generic, homogeneous bianisotropic medium is described using the constitutive relations given in Eq.3. By writing electromagnetic fields inside the material as $[\mathbf{E}, \sqrt{\frac{\mu_0}{\epsilon_0}} \mathbf{H}]^T e^{i(\mathbf{k}_{\parallel} \cdot \mathbf{R} + k_z z - i\omega t)}$ and using these constitutive relations in Maxwell's equations, we obtain the following dimensionless dispersion equation for waves inside the material:

$$\det(M + M_k) = 0, \text{ for } M = \begin{bmatrix} \bar{\bar{\epsilon}} & \bar{\bar{\xi}} \\ \bar{\bar{\zeta}} & \bar{\bar{\mu}} \end{bmatrix}, M_k = \begin{bmatrix} 0 & \bar{\mathbf{k}}/k_0 \\ -\bar{\mathbf{k}}/k_0 & 0 \end{bmatrix}$$

$$\bar{\mathbf{k}} = \begin{bmatrix} 0 & -k_z & k_{\parallel} \sin \phi \\ k_z & 0 & -k_{\parallel} \cos \phi \\ -k_{\parallel} \sin \phi & k_{\parallel} \cos \phi & 0 \end{bmatrix} \quad (21)$$

Here, 6×6 material tensor M describes the constitutive relations and M_k corresponds to the curl operator acting on plane waves. \mathbf{k}_{\parallel} is the parallel component of the incident wave which is conserved at each interface and hence is the same for all layers. k_z is the z -component of the wavevector which is obtained by solving the above equation for given $k_{\parallel} = |\mathbf{k}_{\parallel}|$, the angle ϕ made by \mathbf{k}_{\parallel} with the x -axis, and the material parameters $\bar{\bar{\epsilon}}, \bar{\bar{\mu}}, \bar{\bar{\xi}}, \bar{\bar{\zeta}}$. The associated fields are the null-space eigenstates of the above dispersion equation. For all media, there are four solutions inside each layer of the planar slab where two solutions correspond to waves going in $+z$ direction and the remaining two correspond to waves going in $-z$ direction.

We now consider the incidence of $\hat{\mathbf{e}}_s$ or $\hat{\mathbf{e}}_p$ polarized light. In vacuum, the polarization vectors $\hat{\mathbf{e}}_{j\pm}$ for $j = s, p$ with \pm denoting waves going along $\pm z$ directions are:

$$\hat{\mathbf{e}}_{s\pm} = \begin{bmatrix} \sin \phi \\ -\cos \phi \\ 0 \end{bmatrix}, \hat{\mathbf{e}}_{p\pm} = \frac{-1}{k_0} \begin{bmatrix} \pm k_z \cos \phi \\ \pm k_z \sin \phi \\ -k_{\parallel} \end{bmatrix} \quad (22)$$

Thus, for an incident $\hat{\mathbf{e}}_{s-}$ polarized light (in the top hemisphere for a planar slab) of unit amplitude, the reflected fields in the same layer are $r_{ss}\hat{\mathbf{e}}_{s+} + r_{ps}\hat{\mathbf{e}}_{p+}$ and the transmitted fields on the other side of the slab are $t_{ss}\hat{\mathbf{e}}_{s-} + t_{ps}\hat{\mathbf{e}}_{p-}$. Inside each layer, the fields are

described in the basis of four (null space) eigenstates using four unknowns. Thus, for a planar slab of N layers, there are $4N + 4$ unknowns including the four reflection and transmission coefficients. These can be readily calculated by using $4(N+1)$ boundary conditions (continuity of E_x, E_y, H_x, H_y fields) for $N+1$ interfaces of the planar geometry. The computational tools to calculate these coefficients are made available on GitHub <https://github.com/chinmayCK/Fresnel> under MIT license.

VI. ACKNOWLEDGMENTS

This work was supported by the US Department of Energy, Office of Basic Energy Science under award number de-sc0017717, DARPA Nascent Light-Matter Interaction program, and the Lillian Gilbreth Postdoctoral Fellowship program at Purdue University (CK).

* ckhandek@purdue.edu

† zjacob@purdue.edu

- [1] C. Wu, N. Arju, G. Kelp, J. A. Fan, J. Dominguez, E. Gonzales, E. Tutuc, I. Brener, and G. Shvets, *Nat. Commun.* **5**, 3892 (2014).
- [2] X. Yin, M. Schaferling, B. Metzger, and H. Giessen, *Nano Lett.* **13**, 6238 (2013).
- [3] S. A. Dyakov, V. A. Semenenko, N. A. Gippius, and S. G. Tikhodeev, *Phys. Rev. B* **98**, 235416 (2018).
- [4] N. Shitrit, I. Yulevich, E. Maguid, D. Ozeri, D. Veksler, V. Kleiner, and E. Hasman, *Science* **340**, 724 (2013).
- [5] S. Wadsworth, P. Clem, E. Branson, and G. Boreman, *Opt. Mater. Exp.* **1**, 466 (2011).
- [6] D. Miller, L. Zhu, and S. Fan, *Proc. Natl. Acad. Sci.* **114**, 4336 (2017).
- [7] L. Zhu and S. Fan, *Phys. Rev. B* **90**, 220301 (2014).
- [8] E. Moncada-Villa, V. Fernández-Hurtado, F. J. García-Vidal, A. García-Martín, and J. C. Cuevas, *Phys. Rev. B* **92**, 125418 (2015).
- [9] I. Latella and P. Ben-Abdallah, *Phys. Rev. Lett.* **118**, 173902 (2017).
- [10] P. Ben-Abdallah, *Phys. Rev. Lett.* **116**, 084301 (2016).
- [11] F. Herz and S.-A. Biehs, *EPL* **127**, 44001 (2019).
- [12] R. M. Abraham Ekeroth, A. García-Martín, and J. C. Cuevas, *Phys. Rev. B* **95**, 235428 (2017).
- [13] L. Zhu, Y. Guo, and S. Fan, *Phys. Rev. B* **97**, 094302 (2018).
- [14] I. Žutić, J. Fabian, and S. Das Sarma, *Rev. Mod. Phys.* **76**, 323 (2004).
- [15] C. Khandekar and Z. Jacob, *New J. Phys.* **21**, 103030 (2019).
- [16] T. Van Mechelen and Z. Jacob, *Optica* **3**, 118 (2016).
- [17] A. Yariv and P. Yeh, *Optical waves in crystals: propagation and control of laser radiation*, Wiley series in pure and applied optics (Wiley, 1984).
- [18] Z. Wang, F. Cheng, T. Winsor, and Y. Liu, *Nanotechnology* **27**, 412001 (2016).

- [19] V. Asadchy, A. Díaz-Rubio, and S. Tretyakov, *Nanophotonics* **7**, 1069 (2018).
- [20] A. Ishimaru, *Electromagnetic Wave Propagation, Radiation, and Scattering: From Fundamentals to Applications*, IEEE Press Series on Electromagnetic Wave Theory (Wiley, 2017).
- [21] G. Armelles, A. Cebollada, A. García-Martín, and M. González, *Adv. Opt. Mater.* **1**, 10 (2013).
- [22] P. Sengupta, C. Khandekar, T. Van Mechelen, R. Rahman, and Z. Jacob, *Phys. Rev. B* **101**, 035412 (2020).
- [23] O. V. Kotov and Y. E. Lozovik, *Phys. Rev. B* **98**, 195446 (2018).
- [24] G. Rodrigue, *Proc. of the IEEE* **76**, 121 (1988).
- [25] A. Pyatakov and A. Zvezdin, *Phys.-Uspekhi* **55**, 557 (2012).
- [26] A. LaForge, A. Frenzel, B. Pursley, T. Lin, X. Liu, J. Shi, and D. Basov, *Phys. Rev. B* **81**, 125120 (2010).
- [27] J.-M. Hu, C.-G. Duan, C.-W. Nan, and L.-Q. Chen, *NPJ Comput. Mater.* **3**, 1 (2017).
- [28] M. Green, *Nano Lett.* **12**, 5985 (2012).
- [29] C. Khandekar and Z. Jacob, *Phys. Rev. Appl.* **12**, 014053 (2019).
- [30] M. F. Maghrebi, A. V. Gorshkov, and J. D. Sau, *Phys. Rev. Lett.* **123**, 055901 (2019).
- [31] M. Reid, O. Miller, A. Polimeridis, A. Rodriguez, E. Tomlinson, and S. Johnson, *arXiv:1708.01985* (2017).
- [32] A. Feigel, *Phys. Rev. Lett.* **92**, 020404 (2004).
- [33] B. Van Tiggelen, G. Rikken, and V. Krstić, *Phys. Rev. Lett.* **96**, 130402 (2006).
- [34] O. J. Birkeland and I. Brevik, *Phys. Rev. E* **76**, 066605 (2007).
- [35] M. Kushwaha, *Surf. Sci. Rep.* **41**, 1 (2001).
- [36] E. Palik, R. Kaplan, R. Gammon, H. Kaplan, R. Wallis, and J. Quinn, *Phys. Rev. B* **13**, 2497 (1976).
- [37] J. Chochol, K. Postava, M. Čada, M. Vanwolleghe, L. Halagačka, J.-F. Lampin, and J. Pištora, *AIP Adv.* **6**, 115021 (2016).
- [38] M. G. Silveirinha and S. I. Maslovski, *Phys. Rev. Lett.* **105**, 189301 (2010).
- [39] J.-J. Greffet and M. Nieto-Vesperinas, *J. Opt. Soc. Am. A* **15**, 2735 (1998).
- [40] A. Ott, P. Ben-Abdallah, and S.-A. Biehs, *Phys. Rev. B* **97**, 205414 (2018).
- [41] S. Barnett, L. Allen, R. Cameron, C. Gilson, M. Padgett, F. Speirits, and A. Yao, *J. Opt.* **18**, 064004 (2016).
- [42] S. Barnett, M. Babiker, and M. Padgett, “Optical orbital angular momentum,” (2017).
- [43] R. Graglia, P. Uslenghi, and R. Zich, *Electromagnetics* **11**, 193 (1991).
- [44] S. A. Tretyakov and A. Sochava, *Int. J. Infra. Millim. Waves* **15**, 829 (1994).
- [45] R. Mueller, *J. Appl. Phys.* **42**, 2264 (1971).
- [46] This software is available on GitHub <https://github.com/chinmayCK/Fresnel> under MIT license.
- [47] G. Bimonte and E. Santamato, *Phys. Rev. A* **76**, 013810 (2007).
- [48] W. Padilla, *Opt. Exp.* **15**, 1639 (2007).
- [49] W. Li and S. Fan, *Opt. Exp.* **26**, 15995 (2018).

Universal spin-resolved thermal radiation laws for nonreciprocal bianisotropic media: Supplementary Materials

Chinmay Khandekar,^{1,*} Farhad Khosravi,² Zhou Li,¹ and Zubin Jacob^{1,†}

¹*Birck Nanotechnology Center, School of Electrical and Computer Engineering,
College of Engineering, Purdue University, West Lafayette, Indiana 47907, USA*

²*Department of Electrical and Computer Engineering,
University of Alberta, Edmonton, Alberta T6G1H9, Canada*

(Dated: June 11, 2020)

We show the derivation of spin-resolved emissivities using Rytov's fluctuational electrodynamics. We provide a universal perspective of spin-resolved thermal-radiation characteristics of bi-layered bianisotropic planar media; an extension of the same analysis for single-layered slabs in the main text. Finally, we derive the closed-form expressions of Fresnel coefficients for a semi-infinite half-space of gyromagnetic medium under specific conditions.

I. FLUCTUATIONAL ELECTRODYNAMIC DERIVATION OF EMISSIVITY

The following basis-independent trace formula for the thermal emission power from an object at temperature T into the external vacuum at temperature T_e in terms of its scattering operator (S) has been derived previously [1–3]:

$$H = \int \frac{d\omega}{2\pi} [\Theta(\omega, T) - \Theta(\omega, T_e)] \text{Tr}\{\mathcal{I} - SS^\dagger\} \quad (1)$$

Substituting the scattering matrix for the planar interface in the basis of RCP ($\hat{\mathbf{e}}_{(+)}$) and LCP ($\hat{\mathbf{e}}_{(-)}$) plane waves, we obtain:

$$H_s = \int \frac{d\omega}{2\pi} [\Theta(\omega, T) - \Theta(\omega, T_e)] \text{Tr}\left\{ \int_0^{k_0=\omega/c} \frac{k_{\parallel} dk_{\parallel}}{(2\pi)^2} \int_0^{2\pi} d\phi \left(\mathcal{I} - \begin{bmatrix} r_{(++)} & r_{(+-)} \\ r_{(-+)} & r_{(--) } \end{bmatrix} \begin{bmatrix} r_{(++)}^* & r_{(-+)}^* \\ r_{(+ -)}^* & r_{(--) }^* \end{bmatrix} \right) \right\} \quad (2)$$

Here H_s is the Poynting flux or heat radiation per unit area of the slab in the normal ($\hat{\mathbf{e}}_z$) direction and $r_{(jk)}$ for $j, k = [+,-]$ denotes the amplitude of j -polarized reflected circularly polarized (CP) wave due to unit amplitude k -polarized incident CP wave. $R_{(jk)} = |r_{(jk)}|^2$ denotes the polarization interconversion reflectance used in the calculation of emissivities and absorptivities. k_{\parallel} is the in-plane wavevector which is related to the vacuum wavevector $k_0 = \omega/c$ as $k_{\parallel} = k_0 \sin \theta$. Using $d\Omega = \sin \theta d\theta d\phi$ and assuming the surrounding to be at $T_e = 0\text{K}$, we obtain:

$$H_s = \int d\omega \int d\Omega \underbrace{[1 - R_{(++)}(\theta, \phi) - R_{(+-)}(\theta, \phi)]}_{\eta_{(+)}(\theta, \phi + \pi)} + \underbrace{[1 - R_{(-+)}(\theta, \phi) - R_{(--) }(\theta, \phi)]}_{\eta_{(-)}(\theta, \phi + \pi)} \frac{I_b(\omega, T)}{2} \cos \theta \quad (3)$$

Here $I_b(\omega, T) = \omega^2 \Theta(\omega, T) / (4\pi^3 c^2)$ is the blackbody radiance at temperature T and $\Theta(\omega, T) = \hbar\omega / [\exp(\hbar\omega/k_B T) - 1]$ is the Planck's function. It follows that the integrand of the above expression reproduces the expression for the emitted power per unit area (dA), per unit frequency $d\omega$ within the solid angle $d\Omega$ given by Eq.1 in manuscript. We note that this derivation is not new and has been presented before for isotropic planar media and in the usual basis of (\mathbf{s}, \mathbf{p})-polarization states [1]. A derivation based on the second kind of fluctuation-dissipation theorem (correlations of underlying fluctuating current densities) can be found for isotropic, dielectric/metallic materials in Ref. [4] and for nonreciprocal gyroelectric or magneto-optic planar media in Ref. [5].

II. UNIVERSAL PERSPECTIVE OF SPIN-RESOLVED THERMAL RADIATION FROM MULTILAYERED SLABS

In the main text, we provided a universal perspective of spin-resolved thermal radiation from finite-thickness planar slabs of many material classes. Here we extend it to the case of multi-layered planar slabs. In figure 3 of the manuscript, we consider spin-resolved thermal emission at frequency ω from a planar slab of thickness $d = 0.5c/\omega$

Universal perspective of thermal spin photonics for reciprocal and nonreciprocal bilayered planar media

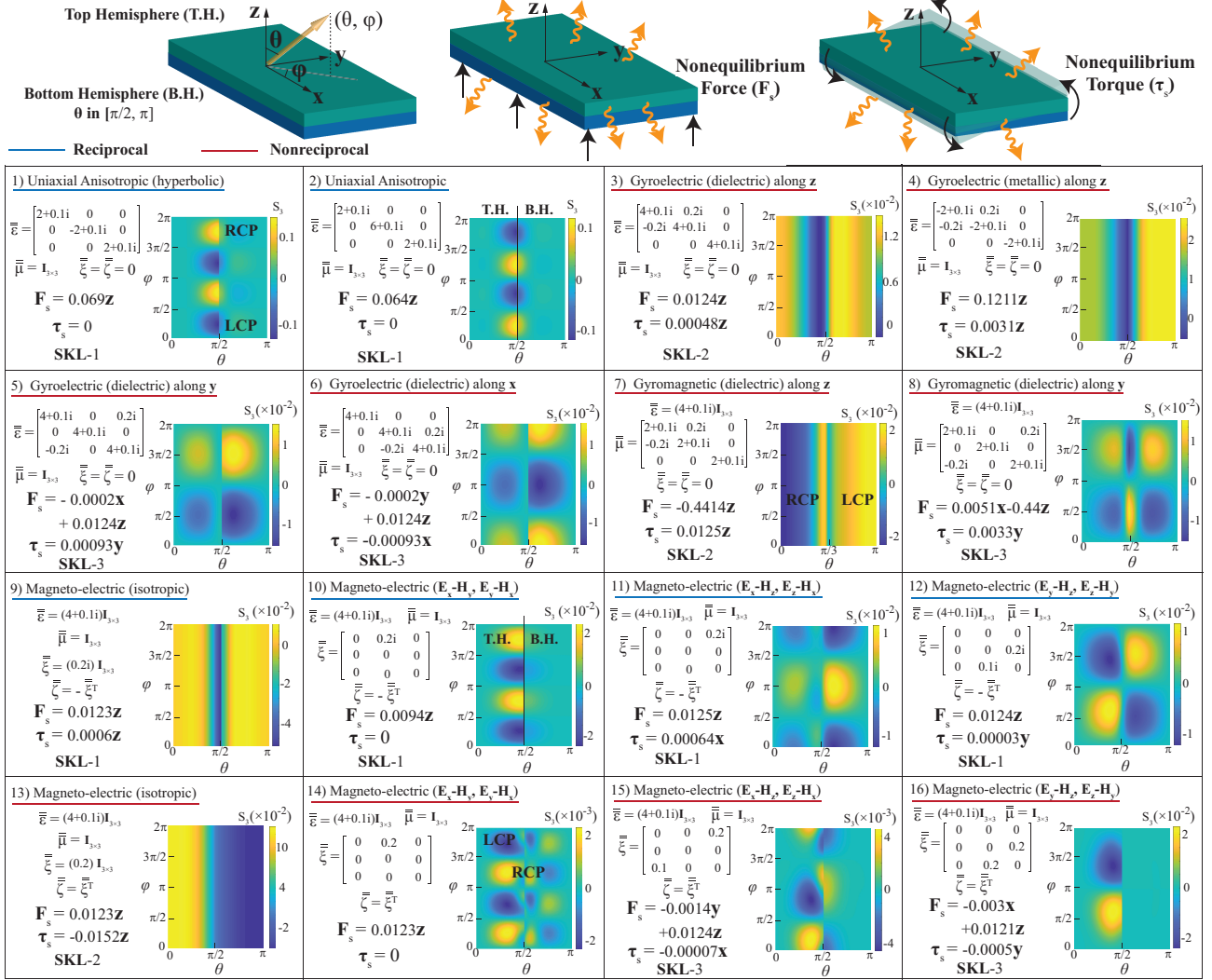


FIG. 1. This figure (an extension of figure 3 in the manuscript) analyzes circularly polarized thermal emission and associated nonequilibrium force and torque for a bi-layered finite-thickness slab. We consider thermal emission at frequency ω from the slab which consists of a bianisotropic material described by $\bar{\epsilon}, \bar{\mu}, \bar{\xi}, \bar{\zeta}$ parameters (top layer having thickness $d = 0.5c/\omega$) on top of a trivial dielectric material of permittivity $\bar{\epsilon} = (8 + 0.1i)\mathcal{I}_{3 \times 3}$ (bottom layer having thickness $d = 0.4c/\omega$). The bi-layered slab at temperature T_0 emits thermal radiation into the surrounding vacuum on both sides at temperature $T = 0\text{K}$. The contour plot in each representative example demonstrates the Stokes S_3 parameter (Eq.??) as a function of (θ, ϕ) which are demonstrated in the top left inset. The calculated spectral force per unit area $\mathbf{F}_s/(I_b T_0/2c)$ and the spectral torque per unit area $\boldsymbol{\tau}_s/(I_b T_0/2\omega)$ arising from the thermal emission from the slab are provided for the given material parameters. The applicable spin-resolved Kirchhoff's law (SKL) is also noted for each example.

containing a bianisotropic medium characterized by the response parameters $\bar{\epsilon}, \bar{\mu}, \bar{\xi}, \bar{\zeta}$. Here, in figure 1, we use the exact same parameters for all examples. But, additionally, we consider the slab to be placed on a dielectric substrate of thickness $d = 0.4c/\omega$ having permittivity $\bar{\epsilon} = (8 + 0.1i)\mathcal{I}_{3 \times 3}$. This asymmetric arrangement (along z -direction) leads to a nonzero spectral thermal force perpendicular to the slab which is otherwise absent for single-layered slabs of most material classes. As explained in the main text, the asymmetric arrangement also leads to a nonzero perpendicular thermal torque for slabs containing isotropic magnetoelectric media (see examples 9,13) where single-layered slabs of these materials do not experience any torque due to symmetric spin-polarized emission in top and bottom hemispheres.

Parallel forces and torques: In the main text, we find that, without using the substrate slab, the parallel nonequilibrium force is experienced only by anisotropic nonreciprocal magnetoelectric materials which cause coupling between perpendicular and parallel components of $\mathbf{E} - \mathbf{H}$ fields (examples 15 and 16). Figure 1 reveals that, in a bi-layered system, gyrotropic media with gyrotropy axis parallel to the surface (examples 5,6,8) also experience a

parallel nonequilibrium force. Furthermore, the above anisotropic magnetoelectric materials (examples 15,16) also experience a parallel nonequilibrium torque that is otherwise absent in a single-layered slab. We note that the parallel forces and torques are both absent for single-layered slabs of anisotropic reciprocal magnetoelectric media (examples 11, 12). However, in a bi-layer system, while the parallel force remains zero, these slabs can experience a torque parallel to the surface. The examples in figure 1 also reveal the dependence of directionalities of nonequilibrium force and torque on the material properties. For example, multilayered planar slabs of gyrotropic media with gyrotropy axis parallel to the surface (examples 5,6,8) experience a torque parallel to the gyrotropy axis and a force which is parallel to the surface but perpendicular to the gyrotropy axis. A multilayered planar slab containing anisotropic nonreciprocal magnetoelectric media that cause coupling of $\mathbf{E}_y - \mathbf{H}_z, \mathbf{E}_z - \mathbf{H}_y$ fields (example 16) experience a force along \mathbf{x} -axis and a torque along \mathbf{y} -axis.

Based on this universal perspective of multilayered bianisotropic slabs which are classified according to the spin-resolved Kirchhoff's laws (**SKLs**), the following general rules can be obtained. They are useful from the perspective of engineering thermal optomechanical forces and torques:

- Perpendicular nonequilibrium thermal force can be obtained for all materials classes.
- Perpendicular nonequilibrium thermal torque can be obtained for nonreciprocal media satisfying **SKL-2** and isotropic reciprocal magnetoelectric media (Pasteur media).
- Parallel nonequilibrium thermal force can exist only for nonreciprocal materials satisfying **SKL-3**.
- Parallel nonequilibrium thermal torque can exist for nonreciprocal media satisfying **SKL-3** and anisotropic reciprocal magnetoelectric media which cause coupling between perpendicular and parallel components of $\mathbf{E} - \mathbf{H}$ fields.

While deriving these rules, we have omitted consideration of multilayered slabs intermixing materials satisfying different **SKLs**. In that case, both perpendicular and parallel components of nonequilibrium force and torque can be engineered.

III. FRESNEL REFLECTION COEFFICIENTS FOR A GYROMAGNETIC HALF-SPACE

We provide semi-analytic closed form expressions of Fresnel reflection coefficients for a gyromagnetic medium and derive some of the interesting relations between them noted in the main text. We consider a semi-infinite half-space of a gyromagnetic material having permittivity $\bar{\epsilon} = \epsilon \mathbf{I}_{3 \times 3}$, and a generic anti-symmetric permeability tensor $\bar{\mu} = \mu_{ij}$ having nonzero off-diagonal elements with the property $\mu_{ij} = -\mu_{ji}$. On the vacuum side of the geometry, we write the incident and reflected electric and magnetic fields as the following:

$$\mathbf{E} = \mathbf{E}^i + \mathbf{E}^r, \quad \mathbf{H} = \mathbf{H}^i + \mathbf{H}^r \quad (4a)$$

$$\mathbf{E}^i = (E_{0s} \hat{s}_- + E_{0p} \hat{p}_-) e^{i\mathbf{k}_- \cdot \mathbf{r}} \quad (4b)$$

$$\mathbf{E}^r = (E_{0s} r_{ss} \hat{s}_+ + E_{0p} r_{pp} \hat{p}_+ + E_{0s} r_{ps} \hat{p}_+ + E_{0p} r_{sp} \hat{s}_+) e^{i\mathbf{k}_+ \cdot \mathbf{r}} \quad (4c)$$

$$\mathbf{H}^i = \frac{1}{\eta_0} (-E_{0s} \hat{p}_- + E_{0p} \hat{s}_-) e^{i\mathbf{k}_- \cdot \mathbf{r}} \quad (4d)$$

$$\mathbf{H}^r = \frac{1}{\eta_0} (-E_{0s} r_{ss} \hat{p}_+ + E_{0p} r_{pp} \hat{s}_+ + E_{0s} r_{ps} \hat{s}_+ - E_{0p} r_{sp} \hat{p}_+) e^{i\mathbf{k}_+ \cdot \mathbf{r}} \quad (4e)$$

where the polarization eigenstates \hat{s}_\pm, \hat{p}_\pm , and the associated wavevectors \hat{k}_\pm/k_0 are:

$$\hat{k}_\pm = k_0 (k_\parallel \cos \phi \hat{x} + k_\parallel \sin \phi \hat{y} \pm k_z \hat{z}), \quad \hat{s}_\pm = \sin \phi \hat{x} - \cos \phi \hat{y}, \quad \hat{p}_\pm = -(\pm k_z \cos \phi \hat{x} \pm k_z \sin \phi - k_\parallel \hat{z}) \quad (5)$$

k_\parallel denotes the conserved wavevector component parallel to the surface and $\eta_0 = \sqrt{\mu_0/\epsilon_0}$. Similarly, we can write the electric and magnetic fields inside the gyromagnetic material as

$$\mathbf{E}' = \mathbf{E}^t, \quad \mathbf{H}' = \mathbf{H}^t \quad (6a)$$

$$\mathbf{E}^t = (E_{0s}t_{ss}\hat{s}'_- + E_{0p}t_{pp}\hat{p}'_- + E_{0s}t_{ps}\hat{p}'_- + E_{0p}t_{sp}\hat{s}'_-) e^{i\mathbf{k}'_- \cdot \mathbf{r}} \quad (6b)$$

$$\bar{\boldsymbol{\mu}}\mathbf{H}^t = \frac{\sqrt{k_{\parallel}^2 + k_z'^2}}{\eta_0} [-E_{0s}t_{ss}\hat{p}'_- + E_{0p}t_{pp}\hat{s}'_- + E_{0s}t_{ps}\hat{s}'_- - E_{0p}t_{sp}\hat{p}'_-] e^{i\mathbf{k}'_- \cdot \mathbf{r}} \quad (6c)$$

where

$$\mathbf{k}'_{\pm} = k_0\hat{k}'_{\pm} = k_0 (k_{\parallel} \cos \phi \hat{x} + k_{\parallel} \sin \phi \hat{y} \pm k'_z \hat{z}), \quad \hat{s}'_{\pm} = \sin \phi \hat{x} - \cos \phi \hat{y}, \quad \hat{p}'_{\pm} = -\frac{\pm k'_z \cos \phi \hat{x} \pm k'_z \sin \phi \hat{y} - k_{\parallel} \hat{z}}{\sqrt{k_{\parallel}^2 + k_z'^2}} \quad (7)$$

Since there is only one interface, we have denoted the transmission coefficients as t_{jk} for $j, k = [s, p]$. Note that $\hat{k}'_{\pm} \times \hat{p}'_{\pm} = \hat{s}'_{\pm}$. The value of k'_z (z -component of the wavevector) inside the medium can be obtained by solving the Maxwell's equations as described in the methods section of the main text. From these solutions and applying the boundary conditions for separate incidence of s -polarized light and p -polarized light, we find the values of r_{ss} , r_{sp} , r_{ps} , r_{pp} for given k_{\parallel} and ϕ . For a gyromagnetic material considered here, the following simplified quartic equation is obtained:

$$a(k'_z)^4 + c(k'_z)^2 + dk'_z + e = 0 \quad (8)$$

where

$$a = \mu_{zz} \quad (9a)$$

$$c = \mu_{zz}k_{\parallel}^2 + \mu_{xx}k_{\parallel}^2 \cos^2 \phi + \mu_{yy}k_{\parallel}^2 \sin^2 \phi - \epsilon\mu_{zz}(\mu_{xx} + \mu_{yy}) - \epsilon\mu_{yz}^2 - \epsilon\mu_{zx}^2 \quad (9b)$$

$$d = 2\epsilon\mu_{xy}k_{\parallel}(\mu_{yz} \cos \phi + \mu_{zx} \sin \phi) \quad (9c)$$

$$e = k_{\parallel}^4 (\mu_{xx} \cos^2 \phi + \mu_{yy} \sin^2 \phi) + \epsilon^2 \mu_{xx} \mu_{yy} \mu_{zz} - \epsilon \mu_{xx} \mu_{yy} k_{\parallel}^2 - \epsilon \mu_{zz} k_{\parallel}^2 (\mu_{xx} \cos^2 \phi + \mu_{yy} \sin^2 \phi) + \epsilon^2 \mu_{xx} \mu_{yz}^2 + \epsilon^2 \mu_{yy} \mu_{zx}^2 + \epsilon^2 \mu_{zz} \mu_{xy}^2 - \epsilon \mu_{xy}^2 k_{\parallel}^2 - \epsilon k_{\parallel}^2 (\mu_{zx} \cos \phi + \mu_{yz} \sin \phi)^2 \quad (9d)$$

There are four solutions where two of them correspond to waves propagating in $-z$ direction and the other two correspond to waves propagating in $+z$ direction. We choose the solutions that correspond to decay of the fields away from the interface inside the medium. Identifying these solutions as $k_z^{(i)}$ with $i = 1, 2$, we have two sets of $t_{ss}^{(i)}$, $t_{sp}^{(i)}$, $t_{ps}^{(i)}$, and $t_{pp}^{(i)}$. Substituting the associated fields in Maxwell's equations, we obtain following equations relating these coefficients by considering x component of the fields:

$$\begin{aligned} & t_{ss}^{(i)} E_{0s} \left[\epsilon \sin \phi + \left(k_z^{(i)} \right)^2 \mu_{xy}^{-1} \cos \phi - \mu_{yy}^{-1} \left(k_z^{(i)} \right)^2 \sin \phi - \mu_{yz}^{-1} k_{\parallel} k_z^{(i)} - \mu_{zx}^{-1} k_{\parallel} k_z^{(i)} \sin \phi \cos \phi + \mu_{yz}^{-1} k_{\parallel} k_z^{(i)} \sin^2 \phi - \mu_{zz}^{-1} k_{\parallel}^2 \sin \phi \right] \\ & + t_{pp}^{(i)} E_{0p} \sqrt{k_{\parallel}^2 + k_z'^{(i)2}} \left[\frac{\epsilon k_z'^{(i)} \cos \phi}{\left(k_{\parallel}^2 + k_z'^{(i)2} \right)} - \mu_{xy}^{-1} k_z'^{(i)} \sin \phi - \mu_{yy}^{-1} k_z'^{(i)} \cos \phi + \mu_{zx}^{-1} k_{\parallel} \sin^2 \phi + \mu_{yz}^{-1} k_{\parallel} \sin \phi \cos \phi \right] \\ & + t_{ps}^{(i)} E_{0s} \sqrt{k_{\parallel}^2 + k_z'^{(i)2}} \left[\frac{\epsilon k_z'^{(i)} \cos \phi}{\left(k_{\parallel}^2 + k_z'^{(i)2} \right)} - \mu_{xy}^{-1} k_z'^{(i)} \sin \phi - \mu_{yy}^{-1} k_z'^{(i)} \cos \phi + \mu_{zx}^{-1} k_{\parallel} \sin^2 \phi + \mu_{yz}^{-1} k_{\parallel} \sin \phi \cos \phi \right] \\ & + t_{sp}^{(i)} E_{0p} \left[\epsilon \sin \phi + \mu_{xy}^{-1} \left(k_z^{(i)} \right)^2 \cos \phi - \mu_{yy}^{-1} \left(k_z^{(i)} \right)^2 \sin \phi - \mu_{yz}^{-1} k_{\parallel} k_z^{(i)} - \mu_{zx}^{-1} k_{\parallel} k_z^{(i)} \sin \phi \cos \phi + \mu_{yz}^{-1} k_{\parallel} k_z^{(i)} \sin^2 \phi - \mu_{zz}^{-1} k_{\parallel}^2 \sin \phi \right] \\ & = 0 \end{aligned} \quad (10)$$

Setting $E_{0p} = 0$ for calculation of r_{ss}, r_{ps} below (incidence of s -polarized light), we obtain:

$$A^{(i)} = \frac{t_{ps}^{(i)}}{t_{ss}^{(i)}} = \frac{\epsilon \sin \phi + \left(k_z^{(i)}\right)^2 \mu_{xy}^{-1} \cos \phi - \mu_{yy}^{-1} \left(k_z^{(i)}\right)^2 \sin \phi - \mu_{yz}^{-1} k_{\parallel} k_z^{(i)} - \mu_{zx}^{-1} k_{\parallel} k_z^{(i)} \sin \phi \cos \phi + \mu_{yz}^{-1} k_{\parallel} k_z^{(i)} \sin^2 \phi - \mu_{zz}^{-1} k_{\parallel}^2 \sin \phi}{\sqrt{k_{\parallel}^2 + k_z^{(i)2}} \left[\frac{\epsilon k_z^{(i)} \cos \phi}{\left(k_{\parallel}^2 + k_z^{(i)2}\right)} - \mu_{xy}^{-1} k_z^{(i)} \sin \phi - \mu_{yy}^{-1} k_z^{(i)} \cos \phi + \mu_{zx}^{-1} k_{\parallel} \sin^2 \phi + \mu_{yz}^{-1} k_{\parallel} \sin \phi \cos \phi \right]} \quad (11)$$

and setting $E_{0s} = 0$ (incidence of p -polarized light), we find:

$$B^{(i)} = \frac{t_{sp}^{(i)}}{t_{pp}^{(i)}} = \frac{1}{A^{(i)}} \quad (12)$$

We also obtain $A^{(i)}$ and $B^{(i)}$ from the \mathbf{y} -component of the fields which are as the following:

$$A^{(i)} = \frac{t_{ps}^{(i)}}{t_{ss}^{(i)}} = \frac{-\epsilon \cos \phi + \left(k_z^{(i)}\right)^2 \mu_{xx}^{-1} \cos \phi + \mu_{xy}^{-1} \left(k_z^{(i)}\right)^2 \sin \phi - \mu_{zx}^{-1} k_{\parallel} k_z^{(i)} + \mu_{zx}^{-1} k_{\parallel} k_z^{(i)} \cos^2 \phi - \mu_{yz}^{-1} k_{\parallel} k_z^{(i)} \sin \phi \cos \phi + \mu_{zz}^{-1} k_{\parallel}^2 \cos \phi}{\sqrt{k_{\parallel}^2 + k_z^{(i)2}} \left[\frac{\epsilon k_z^{(i)} \sin \phi}{\left(k_{\parallel}^2 + k_z^{(i)2}\right)} - \mu_{xx}^{-1} k_z^{(i)} \sin \phi + \mu_{xy}^{-1} k_z^{(i)} \cos \phi - \mu_{zx}^{-1} k_{\parallel} \sin \phi \cos \phi - \mu_{yz}^{-1} k_{\parallel} \cos^2 \phi \right]} \quad (13)$$

$$B^{(i)} = \frac{t_{sp}^{(i)}}{t_{pp}^{(i)}} = \frac{1}{A^{(i)}} \quad (14)$$

We now write the boundary conditions for electric fields.

$$\hat{x} : E_{0s} \sin \phi (1 + r_{ss}) + E_{0p} k_z \cos \phi (1 - r_{pp}) - E_{0s} r_{ps} k_z \cos \phi + E_{0p} r_{sp} \sin \phi = \sum_{i=1}^2 \left[E_{0s} t_{ss}^{(i)} \sin \phi + \frac{E_{0p} t_{pp}^{(i)} k_z^{(i)} \cos \phi}{\sqrt{k_{\parallel}^2 + k_z^{(i)2}}} + \frac{E_{0s} t_{ps}^{(i)} k_z^{(i)} \cos \phi}{\sqrt{k_{\parallel}^2 + k_z^{(i)2}}} + E_{0p} t_{sp}^{(i)} \sin \phi \right] \quad (15a)$$

$$\hat{y} : -E_{0s} \cos \phi (1 + r_{ss}) + E_{0p} k_z \sin \phi (1 + r_{pp}) - E_{0s} r_{ps} k_z \sin \phi - E_{0p} r_{sp} \cos \phi = \sum_{i=1}^2 \left[-E_{0s} t_{ss}^{(i)} \cos \phi + \frac{E_{0p} t_{pp}^{(i)} k_z^{(i)} \sin \phi}{\sqrt{k_{\parallel}^2 + k_z^{(i)2}}} + \frac{E_{0s} t_{ps}^{(i)} k_z^{(i)} \sin \phi}{\sqrt{k_{\parallel}^2 + k_z^{(i)2}}} - E_{0p} t_{sp}^{(i)} \cos \phi \right]. \quad (15b)$$

The boundary conditions for the magnetic field are:

$$\hat{x} : E_{0s} k_z \cos \phi (1 - r_{ss}) - E_{0p} \sin \phi (1 + r_{pp}) - E_{0s} r_{ps} \sin \phi - E_{0p} r_{sp} k_z \cos \phi = \sum_{i=1}^2 \left\{ \mu_{xx}^{-1} \left[E_{0s} t_{ss}^{(i)} k_z^{(i)} \cos \phi - E_{0p} t_{pp}^{(i)} \sqrt{k_{\parallel}^2 + k_z^{(i)2}} \sin \phi - E_{0s} t_{ps}^{(i)} \sqrt{k_{\parallel}^2 + k_z^{(i)2}} \sin \phi + E_{0p} t_{sp}^{(i)} k_z^{(i)} \cos \phi \right] + \mu_{xy}^{-1} \left[E_{0s} t_{ss}^{(i)} k_z^{(i)} \sin \phi + E_{0p} t_{pp}^{(i)} \sqrt{k_{\parallel}^2 + k_z^{(i)2}} \cos \phi + E_{0s} t_{ps}^{(i)} \sqrt{k_{\parallel}^2 + k_z^{(i)2}} \cos \phi + E_{0p} t_{sp}^{(i)} k_z^{(i)} \sin \phi \right] + \mu_{xz}^{-1} \left[E_{0s} t_{ss}^{(i)} k_{\parallel} + E_{0p} t_{sp}^{(i)} k_{\parallel} \right] \right\} \quad (16a)$$

$$\begin{aligned}
\hat{y} : E_{0s}k_z \sin \phi(1 - r_{ss}) + E_{0p} \cos \phi(1 + r_{pp}) + E_{0s}r_{ps} \cos \phi - E_{0p}r_{sp}k_z \sin \phi = \\
\sum_{i=1}^2 \left\{ \mu_{yx}^{-1} \left[E_{0s}t_{ss}^{(i)}k_z'^{(i)} \cos \phi - E_{0p}t_{pp}^{(i)}\sqrt{k_{\parallel}^2 + k_z'^{(i)2}} \sin \phi - E_{0s}t_{ps}^{(i)}\sqrt{k_{\parallel}^2 + k_z'^{(i)2}} \sin \phi + E_{0p}t_{sp}^{(i)}k_z'^{(i)} \cos \phi \right] \right. \\
+ \mu_{yy}^{-1} \left[E_{0s}t_{ss}^{(i)}k_z'^{(i)} \sin \phi + E_{0p}t_{pp}^{(i)}\sqrt{k_{\parallel}^2 + k_z'^{(i)2}} \cos \phi + E_{0s}t_{ps}^{(i)}\sqrt{k_{\parallel}^2 + k_z'^{(i)2}} \cos \phi + E_{0p}t_{sp}^{(i)}k_z'^{(i)} \sin \phi \right] \\
\left. + \mu_{yz}^{-1} \left[E_{0s}t_{ss}^{(i)}k_{\parallel} + E_{0p}t_{sp}^{(i)}k_{\parallel} \right] \right\}
\end{aligned} \tag{16b}$$

with μ_{ij}^{-1} being the elements of the inverse of $\bar{\mu}$ matrix assuming that it is invertible. We get from the electric field's boundary conditions, taking $E_{0p} = 0$ (incidence of \mathbf{s} -polarized light),

$$1 + r_{ss} = \sum_{i=1}^2 t_{ss}^{(i)}, \quad k_z r_{ps} = - \sum_{i=1}^2 \frac{k_z'^{(i)} t_{ps}^{(i)}}{\sqrt{k_{\parallel}^2 + k_z'^{(i)2}}} = - \sum_{i=1}^2 \frac{k_z'^{(i)} A^{(i)} t_{ss}^{(i)}}{\sqrt{k_{\parallel}^2 + k_z'^{(i)2}}} \tag{17}$$

and, taking $E_{0s} = 0$ (incidence of \mathbf{p} -polarized light),

$$k_z(1 - r_{pp}) = \sum_{i=1}^2 \frac{t_{pp}^{(i)} k_z'^{(i)}}{\sqrt{k_{\parallel}^2 + k_z'^{(i)2}}}, \quad r_{sp} = \sum_{i=1}^2 t_{sp}^{(i)} = \sum_{i=1}^2 t_{pp}^{(i)} B^{(i)}. \tag{18}$$

On the other hand, we get from the boundary conditions of the magnetic field, setting $E_{0p} = 0$ (incidence of \mathbf{s} -polarized light),

$$\begin{aligned}
\sum_{i=1}^2 \left[a_s^{(i)} t_{ss}^{(i)} + 2k_z \cos \phi \right] &= 0 \\
\sum_{i=1}^2 \left[b_s^{(i)} t_{ss}^{(i)} + 2k_z \sin \phi \right] &= 0
\end{aligned} \tag{19}$$

where

$$\begin{aligned}
a_s^{(i)} &= - \cos \phi \left[k_z + \mu_{xx}^{-1} k_z'^{(i)} + \sqrt{k_{\parallel}^2 + k_z'^{(i)2}} A^{(i)} \mu_{xy}^{-1} \right] \\
&- \sin \phi \left[- \frac{k_z'^{(i)}}{k_z \sqrt{k_{\parallel}^2 + k_z'^{(i)2}}} A^{(i)} + k_z'^{(i)} \mu_{xy}^{-1} - \sqrt{k_{\parallel}^2 + k_z'^{(i)2}} \mu_{xx}^{-1} A^{(i)} \right] - k_{\parallel} \mu_{xz}^{-1}
\end{aligned} \tag{20}$$

$$\begin{aligned}
b_s^{(i)} &= - \sin \phi \left[k_z + \sqrt{k_{\parallel}^2 + k_z'^{(i)2}} \mu_{xy}^{-1} A^{(i)} + \mu_{yy}^{-1} k_z'^{(i)} \right] \\
&+ \cos \phi \left[- \frac{k_z'^{(i)}}{k_z \sqrt{k_{\parallel}^2 + k_z'^{(i)2}}} A^{(i)} + k_z'^{(i)} \mu_{xy}^{-1} - \sqrt{k_{\parallel}^2 + k_z'^{(i)2}} \mu_{yy}^{-1} A^{(i)} \right] - k_{\parallel} \mu_{yz}^{-1}
\end{aligned} \tag{21}$$

Also, setting $E_{0s} = 0$ (incidence of \mathbf{p} -polarized light), we get:

$$\begin{aligned}
\sum_{i=1}^2 \left[a_p^{(i)} t_{pp}^{(i)} - 2 \sin \phi \right] &= 0 \\
\sum_{i=1}^2 \left[b_p^{(i)} t_{pp}^{(i)} + 2 \cos \phi \right] &= 0
\end{aligned} \tag{22}$$

where

$$a_p^{(i)} = -\sin \phi \left[-\frac{k_z'^{(i)}}{k_z \sqrt{k_{\parallel}^2 + k_z'^{(i)2}} - \sqrt{k_{\parallel}^2 + k_z'^{(i)2}} \mu_{xx}^{-1} + \mu_{xy}^{-1} B^{(i)} k_z'^{(i)}} \right] \quad (23)$$

$$- \cos \phi \left[B^{(i)} k_z + B^{(i)} k_z'^{(i)} \mu_{xx}^{-1} + \sqrt{k_{\parallel}^2 + k_z'^{(i)2}} \mu_{xy}^{-1} \right] - B^{(i)} k_{\parallel} \mu_{xx}^{-1}$$

$$b_p^{(i)} = \cos \phi \left[-\frac{k_z'^{(i)}}{k_z \sqrt{k_{\parallel}^2 + k_z'^{(i)2}} + \mu_{xy}^{-1} k_z'^{(i)} B^{(i)} - \sqrt{k_{\parallel}^2 + k_z'^{(i)2}} \mu_{yy}^{-1}} \right] \quad (24)$$

$$- \sin \phi \left[B^{(i)} k_z + B^{(i)} k_z'^{(i)} \mu_{yy}^{-1} + \sqrt{k_{\parallel}^2 + k_z'^{(i)2}} \mu_{xy}^{-1} \right] - B^{(i)} k_{\parallel} \mu_{yy}^{-1}$$

Solving these equations by substituting the values of $A^{(i)}, B^{(i)}$, we find the coefficients $t_{ss}^{(i)}$ and $t_{pp}^{(i)}$ from which the required reflection coefficients are obtained. Below, we look at specific cases that allow further simplification of these expressions and lead to useful relations between the reflection coefficients.

A. Gyromagnetic slab with gyrotropy axis perpendicular to surface

We calculate the coefficients for light incidence in the \mathbf{xz} -plane such that $\phi = 0$ in the expressions obtained in previous section. This leads to simplified closed-form expressions for reflection coefficients. For a gyromagnetic slab with gyrotropy axis along \mathbf{z} axis, the only nonzero components of the $\bar{\mu}$ tensor are $\mu_{xx} = \mu_{yy}$, μ_{zz} and $\mu_{xy} = -\mu_{yx}$. We also have $\mu_{xx}^{-1} = \mu_{yy}^{-1} = \frac{\mu_{xx}}{\mu_{xx}^2 + \mu_{xy}^2}$, $\mu_{xy}^{-1} = \frac{\mu_{xy}}{\mu_{xx}^2 + \mu_{xy}^2}$, and $\mu_{zz}^{-1} = \frac{1}{\mu_{zz}}$. Defining

$$U^{(i)} = k_z + \mu_{xx}^{-1} k_z^{(i)'} + \sqrt{k_{\parallel}^2 + k_z^{(i)'}2} A^{(i)} \mu_{xy}^{-1} \quad (25)$$

$$V^{(i)} = -\frac{k_z^{(i)'}}{k_z \sqrt{k_{\parallel}^2 + k_z^{(i)'}2}} A^{(i)} + k_z^{(i)'} \mu_{xy}^{-1} - \sqrt{k_{\parallel}^2 + k_z^{(i)'}2} \mu_{xx}^{-1} A^{(i)}$$

and taking $\phi = 0$ (incidence in \mathbf{xz} -plane), we have:

$$r_{ps} = -\frac{2}{V^{(2)}U^{(1)} - V^{(1)}U^{(2)}} \left[\frac{k_z'^{(1)} A^{(1)} V^{(2)}}{\sqrt{k_{\parallel}^2 + k_z'^{(1)2}}} - \frac{k_z'^{(2)} A^{(2)} V^{(1)}}{\sqrt{k_{\parallel}^2 + k_z'^{(2)2}}} \right] \quad (26a)$$

$$r_{sp} = \frac{2}{V^{(2)}U^{(1)} - V^{(1)}U^{(2)}} \left[U^{(2)} - U^{(1)} \right] \quad (26b)$$

From Eqs. (11) and (13), it follows after substituting $\phi = 0$ that,

$$A^{(i)} = \frac{\epsilon - \mu_{zz}^{-1} k_{\parallel}^2 - \mu_{xx}^{-1} k_z'^{(i)2}}{\mu_{xy}^{-1} k_z'^{(i)} \sqrt{k_{\parallel}^2 + k_z'^{(i)2}}} = -\frac{k_z'^{(i)} \mu_{xy}^{-1}}{\frac{\epsilon}{\sqrt{k_{\parallel}^2 + k_z'^{(i)2}} - \sqrt{k_{\parallel}^2 + k_z'^{(i)2}} \mu_{xx}^{-1}}} \quad (27)$$

From these expressions and using Eqs. (17) and (18) we find:

$$r_{sp} = \frac{2}{V^{(2)}U^{(1)} - V^{(1)}U^{(2)}} \frac{k_z'^{(1)} - k_z'^{(2)}}{k_z'^{(1)} k_z'^{(2)}} \left(\epsilon - \mu_{zz}^{-1} k_{\parallel}^2 \right) \quad (28)$$

and

$$r_{ps} = \frac{2}{V^{(2)}U^{(1)} - V^{(1)}U^{(2)}} \frac{A^{(1)}A^{(2)}}{\sqrt{k_{\parallel}^2 + k_z'^{(1)2}} \sqrt{k_{\parallel}^2 + k_z'^{(2)2}}} \epsilon \left(k_z'^{(1)} - k_z'^{(2)} \right) \quad (29)$$

In the case when the magnetic field is along one of the axes of the problem, the parameter d in Eq. (9c) becomes zero and Eq. (8) becomes a simple second order equation. Using its solutions, and taking $\phi = 0$, we find the following relations to hold true:

$$k_z'^{(1)2} k_z'^{(2)2} = (\epsilon - k_{\parallel}^2 \mu_{zz}^{-1}) \left[\epsilon (\mu_{xy}^2 + \mu_{xx}^2) - \mu_{xx} k_{\parallel}^2 \right] \quad (30a)$$

$$\left(k_{\parallel}^2 + k_z'^{(1)2} \right) \left(k_{\parallel}^2 + k_z'^{(2)2} \right) = \left(\epsilon - k_{\parallel}^2 \mu_{zz}^{-1} \right) \epsilon \left(\mu_{xx}^2 + \mu_{xy}^2 \right) + \mu_{xx} \epsilon k_{\parallel}^2 \quad (30b)$$

$$k_z'^{(1)2} + k_z'^{(2)2} = \mu_{xx} \epsilon + \mu_{xx} \left(\epsilon - \mu_{zz}^{-1} k_{\parallel}^2 \right) - k_{\parallel}^2 \quad (30c)$$

Using these relations and using the first equality of Eq. (27), we obtain:

$$\frac{A^{(1)}A^{(2)}}{\sqrt{k_{\parallel}^2 + k_z'^{(1)2}} \sqrt{k_{\parallel}^2 + k_z'^{(2)2}}} = \frac{\epsilon - \mu_{zz}^{-1} k_{\parallel}^2}{\epsilon k_z'^{(1)} k_z'^{(2)}} \quad (31)$$

Plugging this into Eq. (29) we find

$$r_{ps}(\theta, \phi = 0) = r_{sp}(\theta, \phi = 0) \quad (32)$$

For the case when $\phi = \pi$, all the equations for $\phi = 0$ remain the same. This means that $r_{sp}(\theta, \phi = 0) = r_{sp}(\theta, \phi = \pi)$. Based on rotational symmetry in \mathbf{xy} plane, it can be argued that this holds true for all angles (θ, ϕ) such that:

$$r_{ps}(\theta, \phi) = r_{ps}(\theta, \phi + \pi) = r_{sp}(\theta, \phi + \pi) \quad (33)$$

Furthermore, it can be shown that

$$t_{ss}^{(2)} = \frac{2k_z V^{(2)}}{V^{(2)}U^{(1)} - V^{(1)}U^{(2)}}, \quad t_{ss}^{(1)} = -\frac{2k_z V^{(1)}}{V^{(2)}U^{(1)} - V^{(1)}U^{(2)}} \quad (34)$$

which is valid for $\phi = 0$ or $\phi = \pi$. This means that, through Eqs. (17) and (18), $r_{ss}(\theta, \phi = 0) = r_{ss}(\theta, \phi = \pi)$ and $r_{pp}(\theta, \phi = 0) = r_{pp}(\theta, \phi = \pi)$. Because of rotational symmetry, the same holds true for other values of ϕ . These relations between the reflection coefficients are useful to derive the second spin-resolved Kirchhoff's law in the main text.

B. Gyromagnetic slab with the gyrotropy axis parallel to the surface

We assume the gyrotropy axis to be along \mathbf{x} axis. In this case the only nonzero components of the $\bar{\bar{\mu}}$ tensor are μ_{xx} , $\mu_{yy} = \mu_{zz}$, and $\mu_{yz} = -\mu_{zy}$. Considering the incidence at arbitrary angle θ but fixed $\phi = 0$, we define:

$$U_x^{(i)} = k_z + \mu_{xx}^{-1} k_z'^{(i)}, \quad V_y^{(i)} = -\frac{k_z'^{(i)} A^i}{k_z \sqrt{k_{\parallel}^2 + k_z'^{(i)2}}} - \sqrt{k_{\parallel}^2 + k_z'^{(i)2}} A^{(i)} \mu_{xx}^{-1} \quad (35)$$

and performing similar analysis as above, we find that:

$$r_{sp} = \frac{-2}{\left(U_x^{(2)} V_y^{(1)} - U_x^{(1)} V_y^{(2)} \right) + k_{\parallel} \mu_{yz}^{-1} \left(U_x^{(1)} - U_x^{(2)} \right)} \left(U_x^{(2)} - U_x^{(1)} \right) \quad (36)$$

and

$$r_{ps} = \frac{2}{\left(U_x^{(2)}V_y^{(1)} - U_x^{(1)}V_y^{(2)}\right) + k_{\parallel}\mu_{yz}^{-1}\left(U_x^{(1)} - U_x^{(2)}\right)} \left[\frac{k_z'^{(1)}A^{(1)}}{\sqrt{k_{\parallel}^2 + k_z'^{(1)2}}}\left(V_y^{(2)} - k_{\parallel}\mu_{yz}^{-1}\right) - \frac{k_z'^{(2)}A^{(2)}}{\sqrt{k_{\parallel}^2 + k_z'^{(2)2}}}\left(V_y^{(1)} - k_{\parallel}\mu_{yz}^{-1}\right) \right]. \quad (37)$$

Simplifying the above expressions, we obtain:

$$r_{sp} = \frac{2}{\left(U_x^{(2)}V_y^{(1)} - U_x^{(1)}V_y^{(2)}\right) + k_{\parallel}\mu_{yz}^{-1}\left(U_x^{(1)} - U_x^{(2)}\right)} \mu_{xx}^{-1}\left(k_z'^{(1)} - k_z'^{(2)}\right) \quad (38)$$

$$r_{ps} = -\frac{2}{\left(U_x^{(2)}V_y^{(1)} - U_x^{(1)}V_y^{(2)}\right) + k_{\parallel}\mu_{yz}^{-1}\left(U_x^{(1)} - U_x^{(2)}\right)} \frac{\epsilon A^{(1)}A^{(2)}}{\sqrt{k_{\parallel}^2 + k_z'^{(1)2}}\sqrt{k_{\parallel}^2 + k_z'^{(2)2}}}\left(k_z'^{(1)} - k_z'^{(2)}\right) \quad (39)$$

Again, we find the following equation holds true:

$$\frac{A^{(1)}A^{(2)}}{\sqrt{k_{\parallel}^2 + k_z'^{(1)2}}\sqrt{k_{\parallel}^2 + k_z'^{(2)2}}} = \frac{\mu_{xx}^{-1}}{\epsilon} \quad (40)$$

This leads to:

$$r_{ps}(\theta, \phi = 0) = -r_{sp}(\theta, \phi = 0) \quad (41)$$

If $\phi = \pi$, we find that:

$$r_{sp} = \frac{2}{\left(U_x^{(2)}V_y^{(1)} - U_x^{(1)}V_y^{(2)}\right) - k_{\parallel}\mu_{yz}^{-1}\left(U_x^{(1)} - U_x^{(2)}\right)} \left(U_x^{(2)} - U_x^{(1)}\right) \quad (42)$$

and

$$r_{ps} = -\frac{2}{\left(U_x^{(2)}V_y^{(1)} - U_x^{(1)}V_y^{(2)}\right) - k_{\parallel}\mu_{yz}^{-1}\left(U_x^{(1)} - U_x^{(2)}\right)} \left[\frac{k_z'^{(1)}A^{(1)}}{\sqrt{k_{\parallel}^2 + k_z'^{(1)2}}}\left(V_y^{(2)} + k_{\parallel}\mu_{yz}^{-1}\right) - \frac{k_z'^{(2)}A^{(2)}}{\sqrt{k_{\parallel}^2 + k_z'^{(2)2}}}\left(V_y^{(1)} + k_{\parallel}\mu_{yz}^{-1}\right) \right]. \quad (43)$$

following the same procedure discussed above, we obtain:

$$r_{ps} = \frac{2}{\left(U_x^{(2)}V_y^{(1)} - U_x^{(1)}V_y^{(2)}\right) - k_{\parallel}\mu_{yz}^{-1}\left(U_x^{(1)} - U_x^{(2)}\right)} \frac{\epsilon A^{(1)}A^{(2)}}{\sqrt{k_{\parallel}^2 + k_z'^{(1)2}}\sqrt{k_{\parallel}^2 + k_z'^{(2)2}}}\left(k_z'^{(1)} - k_z'^{(2)}\right) \quad (44)$$

Eq. (40) still holds for $\phi = \pi$. Therefore, we get

$$r_{ps}(\theta, \phi = \pi) = -r_{sp}(\theta, \phi = \pi) \quad (45)$$

When $\phi = \pi/2$, the denominator in Eq. (11) and the numerator in Eq. (13) become zero. In this case,

$$k_z^{(1)'}{}^2 = \frac{\epsilon}{\mu_{xx}^{-1}} - k_{\parallel}^2, \quad k_z^{(2)'}{}^2 = \frac{\epsilon}{\mu_{yy}} - k_{\parallel}^2 \quad (46)$$

Using these relations, we find that $t_{ss}^{(1)} = t_{sp}^{(1)} = t_{pp}^{(2)} = t_{ps}^{(2)} = 0$. On the other hand, we get from Eqs. (19) and (22) that $t_{sp}^{(2)} = t_{ps}^{(1)} = 0$. This means that the only non-zero transmission coefficients are $t_{ss}^{(2)}$ and $t_{pp}^{(1)}$ and substituting these coefficients, we get

$$r_{sp}(\theta, \phi = \pi/2) = r_{ps}(\theta, \phi = \pi/2) = 0 \quad (47)$$

While we prove the above conditions analytically, for other values of ϕ , we have to rely on numerical approach. Interestingly, the condition $r_{sp}(\theta, \phi) = -r_{ps}(\theta, \phi)$ holds true for all angles. This condition is used to derive the third spin-resolved Kirchhoff's law.

While we provide one example here, it is impractical to derive the closed-form expressions of Fresnel coefficients for arbitrary incidence angles (θ, ϕ) for each bianisotropic material class. The generic expressions are evidently complicated (see above) because of the nontrivial dependence of the wavevector and the plane wave solutions inside each such medium on many parameters and often through conditional expressions (real or complex roots of quartic polynomials). Furthermore, such closed form expressions, if obtained, cannot be readily extended to describe a composite medium such as a material which is simultaneously gyrotropic and magnetoelectric. The task of obtaining the closed-form expressions for both reflection and transmission coefficients for a multilayered planar slab becomes more complicated because it involves solving the boundary conditions at many interfaces rather than a single interface for the half-space geometry. Because of these reasons, we have undertaken a more practical alternative of using exact numerical methods to obtain the Fresnel coefficients for arbitrary angles of incidence and for generic multilayered or composite planar slabs. The various relations between the reflection and transmission coefficients discovered using this numerical approach are noted in the manuscript.

* ckhandek@purdue.edu

† zjacob@purdue.edu

- [1] M. Krüger, G. Bimonte, T. Emig, and M. Kardar, "Trace formulas for nonequilibrium casimir interactions, heat radiation, and heat transfer for arbitrary objects," *Phys. Rev. B* **86**, 115423 (2012).
- [2] M. F. Maghrebi, R. L. Jaffe, and M. Kardar, "Spontaneous emission by rotating objects: A scattering approach," *Phys. Rev. Lett.* **108**, 230403 (2012).
- [3] G. Bimonte, "Scattering approach to casimir forces and radiative heat transfer for nanostructured surfaces out of thermal equilibrium," *Phys. Rev. A*. **80**, 042102 (2009).
- [4] K. Joulain, J-P. Mulet, F. Marquier, R. Carminati, and J.-J. Greffet, "Surface electromagnetic waves thermally excited: Radiative heat transfer, coherence properties and casimir forces revisited in the near field," *Surf. Sci. Rep.* **57**, 59–112 (2005).
- [5] E. Moncada-Villa, V. Fernández-Hurtado, F. J. García-Vidal, A. García-Martín, and J. C. Cuevas, "Magnetic field control of near-field radiative heat transfer and the realization of highly tunable hyperbolic thermal emitters," *Phys. Rev. B* **92**, 125418 (2015).